FUTURE VARIABILITY IN ARCTIC SEA ICE

WITH AN ANALYSIS OF A MARINE TRANSPORTATION INDEX

by

Collin E. Tuttle

A thesis submitted in partial fulfilment of

the requirements for the degree of

Master of Science

(Atmospheric and Oceanic Sciences)

at the

UNIVERSITY OF WISCONSIN-MADISON

2018

Thesis Declaration and Approval

I, Collin Tuttle, declare that this thesis titled "Future Variability in Arctic Sea Ice with an Analysis of a Marine Transportation Index" and the work presented in it are my own.

Collin Tuttle	Collin Tuttle	May 31, 2018
Author	Signature	Date

I hereby approve and recommend for acceptance this work, in partial fulfillment of the requirements for the degree of Master of Science:

Dr. Steve Vavrus	Stephen Vavrus	6/1/2018
Committee Chair	Signature	Date
Dr. Dan Vimont	Daniel J. Vimont	5/31/2018
Faculty Member	Signature	Date
Dr. Tristan L'Ecuyer	Tristan L'Ecuyer	6/8/2018
Faculty Member	Signature	Date

Abstract

The recent dramatic loss of Arctic sea ice has fostered a growing interest in the commercial usage of the region. September, the peak of the Arctic marine navigation season, has lost over 60% of its sea ice volume, which has fostered an opportunity for an increase of marine usage. With September sea ice extents predicted to disappear by mid-century, several studies have indicated that polar shipping routes will be more beneficial than traditional Panama and Suez Canal routes. A key gap from previous work on sea ice projections has been a thorough investigation of sea ice interannual variability and its impact on marine usage of the Arctic. Here, we used 40 realizations of a fully-coupled global climate model to investigate trends in sea ice variability. We determined that there is an increase in future variability of multiple sea ice metrics that occurs simultaneously with an increasing rate of ice loss. The Ice Numeral (IN), a metric designed to assess marine navigability, similarly showed an increase in future interannual variability. While the trend of IN clearly indicates a progression to open shipping lanes, there will also be some compensation from reduced reliability due to increased interannual variability of IN in the future. Additionally, it was found that interannual variability took a unique shape for each metric, and that the timing of peak IN variability differs by season. Finally, IN for a vessel with no ice-strengthening was found to align closely with sea ice concentration, while IN for an ice-strengthened vessel aligned more closely with sea ice thickness.

Dedication

i. *To my daughter, Juliette. Let your curiosity exceed my own.*

ii. *To the long history of Coasties who pursued service of both science and country, from Admiral "Iceberg" Smith to the next generation of Cadet "fish kissers." Keep up the good fight!*

Acknowledgements

This work has been made possible by the contributions of so many. First, I would like to thank my advisor, Dr. Steve Vavrus, for his insight and constant input. I am indebted to many members of the faculty who played instrumental roles in my admission to this department as well as for their mentoring and feedback, including Dr. Galen McKinley, Dr. Dan Vimont, Dr. Tristan L'Ecuyer, and Dr. Ankur Desai. Additionally, I have learned (and so often depended on) so much from members of my research groups and peers in the department, including John Mioduszewski, Sean Ridge, Lucas Gloege, Andrew Dzambo, CJ Begalke, and many others! I am thankful for the opportunity to pursue a master's degree provided to me by the US Coast Guard; this job has never been dull, and I am beyond grateful for the incredible diverse career these 10 years have bestowed on me (including the chance to grow a beard and wear normal people clothes). Finally, I could not have accomplished this without the unending support of my wife, Judi.

Table of Contents

List of Tables

List of Abbreviations

AIRSS	Arctic Ice Regime Shipping System
AIS	Automatic Identification System
CAM	Community Atmosphere Model
CCSM	Community Climate System Model
CESM	Community Earth System Model
CICE	Sea Ice Code
CMIP	Coupled Model Inter-Comparison Project
DMSP	Defense Meteorological Satellite Program
GCM	Global Climate Model
GWN	Gaussian White Noise
IM	Ice Multiplier
IN	Ice Numeral
LENS	Large Ensemble
LNG	Liquid Natural Gas
NCAR	National Center for Atmospheric Research
NEP	Northeast Passage
NSR	Northern Sea Route
NWP	Northwest Passage
OW	Open Water class vessel
PC6	Polar Class 6 vessel
PIOMAS	Pan-Arctic Ice Ocean Modelling and Assimilation System
RCP	Representative Concentration Pathway
SIA	Sea Ice Area
SIC	Sea Ice Concentration
SIE	Sea Ice Extent
SIT	Sea Ice Thickness
SIV	Sea Ice Volume
SMMR	Scanning Multi-Channel Microwave Radiometer
SSM/I	Special Sensor Microwave Imagers
SSMIS	Special Sensor Microwave Imager/Sounders
TSR	Transpolar Sea Route

1. Introduction

Recent anthropogenic warming of the Earth's climate has had striking impacts on the polar regions. The Arctic has shown to be a particularly sensitive area, warming at a pace double that of the global average; which has often been termed as "Arctic amplification" (Overland et al., 2017). This has resulted in a significant perturbation to the natural state of the Arctic sea ice cover, namely, the rapid loss of sea ice. In addition to implications for the physical state of the Arctic, the changes are increasingly more relevant for human activities. It is not obvious how these changes will affect sea ice *variability*, although previous work has found increased variability associated with specific sea ice extents, this study will delve further into the question (Goosse et al., 2009). Particularly, the effect that variability changes on interannual timescales might have on marine shipping, which has a growing potential for expansion into the region, will be analyzed.

Arctic Amplification

The increase to the atmospheric carbon reservoir has driven a warming with a variety of feedbacks and responses, one of which being that the Arctic warms at a pace greater than the global average; this is referred to as Arctic amplification. Notably, the ice-albedo feedback is one of the most important feedbacks driving this amplification (Cao et al., 2015; Pithan & Mauritsen, 2014). This process stems primarily from the loss of Arctic sea ice, due to a warmer atmosphere and ocean. In

turn, the loss of highly reflective sea ice increases the area of dark ocean. As shown by Perovich (2002), the albedo of sea ice can range from 0.6 (bare ice) to 0.9 (dry snow cover). Contrasting this, the open ocean can have an albedo as low as 0.03 (Jin, 2004). The increased absorption of incoming solar radiation as sea ice melts enhances the warming from the planet's initial greenhouse forcing. Regionally, this is one of the most important factors driving Arctic amplification. However, several other important factors contribute to the amplification such as the lapse rate and Planck feedbacks, as shown by Pithan and Mauritsen (2014).

Ice Loss in Recent Decades

Sea ice loss has manifested both in extent and volume. The loss rate has changed throughout the past few decades, as well as displaying differing trends across months and seasons. The months of March and September typically represent the annual extremes for sea ice coverage and will be frequently referred to in this paper for that reason. Between the 1979-1984 and 2013-2017 periods, sea ice extent (SIE) decreased by 9% and 33% for March and September, respectively (Table 1) (Fetterer et al., 2017). September SIE has seen a much greater decrease and a loss rate that has grown faster than winter ice. From 1979-2000 the SIE loss in March and September was 0.3% per year and 0.7% per year, respectively (Meier et al., 2014). From 2001-2013 the rate of March SIE loss decreased to 0.2% per year, while September's rate ballooned to 3% per year. Figure 1 displays the September

median SIE from 1981-2010, alongside the observational record minimum, 2012 (Fetterer et al., 2017; Jakobsson et al., 2012).

Thickness and volume loss are closely related to the change in distribution of ice age. Old ice is typically thicker than young ice and can hold a disproportionate amount of ice mass. Maslanik et al. (2011) utilized a satellite-derived ice age product to track the changes in the spatial distribution of ice age. For the month of March, it was found that multiyear ice (survived at least one thawing cycle) went from 75% of the total extent in 1980 to only 45% in 2011. While the loss of old ice implies a loss of ice volume, it is more difficult to quantify, because thickness observations are sparse both temporally and spatially. Estimates of ice volume loss have been obtained through the Pan-Arctic Ice Ocean Modeling and Assimilation System (PIOMAS) and from CryoSat and ICESat observations (Schweiger et al., 2011; Zhang & Rothrock, 2003). The volume loss between the periods of 1979-1984 and 2013-2017 was 28% in March and 63% in September (Table 1) (Schweiger et al., 2011).

Table 1: Ice Loss in Recent Decades

	SIE[a] (million km^2)		Volume[b] (1000 km^3)	
	March	September	March	September
1979-84	16.03	7.31	30	14.95
2013-17	14.57	4.87	21.62	5.5
Diff	-1.46	-2.44	-8.38	-9.45
% Loss	**9%**	**33%**	**28%**	**63%**

[a]Fetterer, F., K. Knowles, W. Meier, M. Savoie, and A. K. Windnagel. 2017, updated daily. *Sea Ice Index, Version 3*. [Sea ice extent]. Boulder, Colorado USA. NSIDC: National Snow and Ice Data Center.
doi: https://doi.org/10.7265/N5K072F8. [February 1, 2018].
[b]Schweiger, A., R. Lindsay, J. Zhang, M. Steele, H. Stern, Uncertainty in modeled arctic sea ice volume, J. Geophys. Res., doi:10.1029/2011JC007084, 2011

Arctic Sea Routes

The opening of the Arctic is of special interest to the commercial marine shipping industry. Commercial traffic largely follows traditional routes around the globe. For transoceanic voyages (Pacific-Atlantic and vice versa) this relies on congested canal routes, such as the Suez and Panama Canals. Additionally, continent-rounding routes force shipping into the often-heavy seas of the Southern Ocean. The Arctic, as a marine corridor, offers significant reductions to both travel time and distance. Specifically, the Northern Sea Route (NSR) reduces up to 47% of the distance of traditional routes (Rodrigue, 2017). Sailing distances, and the reductions from Arctic routes are displayed in Table 2.

The Arctic Ocean contains three major routes, each of which provides a different degree of accessibility. Figure 1 shows the three idealized routes discussed here, taken from Ellis and Brigham (2009). The Northwest Passage (NWP) rounds North

America and transits through the Canadian archipelago and the Davis Strait. Of note, the NWP encompasses several passages and offshoots that navigate the 36,000 islands in the archipelago (Ellis & Brigham, 2009). Each individual passage has a unique constraint to depth and channel width. Because of the number of islands, some of the oldest and thickest ice in the Arctic can be found within the confines of the NWP (Wadhams, 2000). Travel from Europe to East Asia by the NWP is approximately 13,600 km (Rodrigue, 2017).

The NSR transits the northern coast of Europe and Asia, most of which is Russian coastline, before exiting the Arctic through the Bering Strait. The NSR is much more established as a navigable route by the Russian government than the NWP is by the Canadian administration, and it receives more traffic as a result (Ellis & Brigham, 2009). This combined route represents a transit of approximately 12,800 km from Europe to Asia (Rodrigue, 2017). The Northeast Passage (NEP) is the portion of the NSR that transits the Kara Sea. Future references in this paper will refer to the combined NSR and NEP simply as the Northern Sea Route.

Finally, there is one additional route, the Transpolar Sea Route (TSR), which passes through the Greenland Sea, the center of the Arctic Basin (near the pole), and through the Bering Strait. This route has been considered in climate projections of shipping routes but is largely hypothetical as it traverses the center of current summer ice extents.

Table 2: Sailing distances from Europe to Asia. NWP/NSR refers to the Northwest Passage/Northern Sea Route.

	Distance[a] (km)	% reduction from	
		Suez	Panama
Suez Canal	21,000	n/a	n/a
Panama Canal	24,000	n/a	n/a
NWP	13,600	**35%**	**43%**
NSR	12,800	**39%**	**47%**

[a]Rodrigue, J-P *et al.* (2017) *The Geography of Transport Systems*, Hofstra University, Department of Global Studies & Geography, https://transportgeography.org.

History and Modern Arctic Commercial Usage

The Arctic has long been of interest to explorers and those seeking trade routes. The NWP was first transited by a ship over the course of three years from 1903-1906 by Roald Amundsen (Ellis & Brigham, 2009). 63 years later it was traversed by a commercial vessel for the first time, the SS Manhattan. The NSR has maintained an interest from the Soviet Union's and Russian governments. Shipping through the NSR peaked in 1987 with 1,306 voyages conducted by 331 vessels (Ellis & Brigham, 2009). This peak in shipping is owed to the efforts of the Soviet Union to keep the route open, and not related to a favorable ice climatology at the time. An average of 38 vessels transited the NSR annually from 2011-2016 (Protection of the Arctic Marine Environment, 2018). The economic viability of the NSR under recent climate conditions was demonstrated recently, as a liquid natural-gas (LNG) tanker became the first vessel to transit unassisted in winter (Darby, 2018).

While commercial interest and usage of the Arctic has been variable through time, the opening of the basin is likely to foster a greater use in the future. A study on traffic from vessel automatic identification system (AIS) by Pizzolato et al. (2016) revealed significant increases to marine usage of the Arctic since 1990.

Ice Numeral

This study will largely utilize a marine shipping metric, the Ice Numeral (IN), which was first prescribed by Transport Canada as part of the Arctic Ice Regime Shipping System (AIRSS) (Timco et al., 2005). The purpose of the IN is to give mariners a simple metric for determining if ice conditions are safe for transiting. The Ice Numeral is of interest for several reasons. First of all, it has a legal basis in the Canadian Arctic, where vessels are mandated to not proceed through certain IN regimes. Secondly, it is a seemingly simple metric that takes into account ice thickness and concentration, but it also has interesting non-linearities apparent when scrutinized. Finally, it has recently received attention from members of the scientific community when investigating the future climatology of polar sea routes (Melia et al., 2016; Smith & Stephenson, 2013; Stephenson & Smith, 2015).

Previous Work

A great deal of research has been focused on the timing of Arctic sea ice loss, as well as the implications for marine transportation. Utilizing seven ensembles members from the Community Climate System Model, version 3 (CCSM3), Holland et al.

(2006) found that September Arctic SIE loss was punctuated by events of rapid ice loss. Under representative concentration pathway (RCP) 8.5 forcing (high greenhouse gas emissions), they also determined that September ice-free conditions could be expected as soon as 2040. Utilizing the Community Earth System Model, version 1 (CESM1) Jahn et al. (2016) sought to answer a similar question. Here, two scenarios were analyzed: RCP8.5 (40 ensembles) and the lower-emissions RCP4.5 (15 ensembles). The internal variability of the model generated a spread in the timing of the first ice-free (SIE < 1 million km^2) summer, which ranged from 2032-2053 for RCP8.5 and 2043-2058 for RCP4.5.

The timing of a seasonally ice-free Arctic also motivated another question: when will Arctic shipping lanes be navigable? Smith and Stephenson (2013) recently tried to answer this question by utilizing the IN with output from seven coupled atmosphere-ocean general circulation models (GCM), under RCPs 4.5 and 8.5. Breaking the model runs into three time periods, 1979-2005, 2006-2015, and 2040-2059, the authors determined the feasibility of vessels with no and moderate ice strengthening (open-water and polar class 6, respectively) transiting each sea route. During the historical period (1979-2005), only the NSR was feasible for either type of vessel, with a success rate of about 40%. However, in the early 21st century, polar class 6 (PC6) vessel transits began to migrate northward under both forcing scenarios. In the mid-century, the NWP became feasible for both vessel types under

both forcing scenarios, and the TSR opened for open-water (OW) vessels under RCP8.5.

In a follow-on study, Stephenson and Smith (2015) investigated the importance of model choice on shipping projections. The authors chose 10 models from the Coupled Model Intercomparison Project (CMIP5) and performed an analysis similar to that of Smith and Stephenson (2013) (Taylor et al., 2012). It was verified that the TSR, the shortest Arctic route, would gradually become more important than the NSR as ice conditions allowed. Most importantly, it was identified that the variance among the 10 models was non-trivial. Simply put, this finding meant that the model chosen for an analysis altered the results, which stems from the unique mechanics, assumptions, and sensitivity of each model.

Melia et al. (2016) performed an analysis similar to those by Stephenson and Smith, but using three ensembles each from five member models (15 realizations total) of CMIP5. A key finding was the reduction in sailing time offered even by the low emission scenario, RCP2.6. On average, a 30-day Suez Canal trip from Europe to East Asia would be lowered to 22 days under RCP2.6 and 17 days under RCP8.5 by the end of the century. Additionally, the authors made note of considerable interannual variability in Arctic sea route accessibility, but little was done to quantify this. Interannual variability is a key concept that impacts the feasibility of Arctic shipping and deserves a more detailed investigation, because variability is inherently tied to

reliability, which is an important factor in the operational planning of shipping strategy.

Purpose of Study

This study seeks to fill knowledge gaps remaining from the notable previous work (Melia et al., 2016; Smith & Stephenson, 2013; Stephenson & Smith, 2015). While much has been done with the IN to determine marine accessibility, the IN itself has not been dissected. Although the IN is a seemingly simple combination of thickness and concentration, the role that each term plays temporally, spatially, and by vessel class is interesting and worth analyzing. Each of the stated factors has a unique effect on IN and the impact to shipping, as will be described in Section 3. Next, we will seek to quantify the interannual variability of key ice metrics in the warming Arctic. The reductions to ice cover and average vessel travel times tell an inviting story for marine shipping. However, superimposed interannual variability is an important additional factor that could affect expectations of navigable shipping lanes. The reduction to sea ice cover is often taken to represent a future that is increasingly more hospitable to transportation. However, while the overall trend in sea ice points towards sea routes that are more open, an increase in variability would mean that sea routes are less reliable, and thus less predictable for planners. The timing and amplitude of interannual variability will be addressed for a variety of sea ice metrics including the IN. Finally, it will be determined how interannual

variability in the IN relates to other sea ice metrics, such as concentration, thickness, area, and volume.

2. Data

2.1. Sea Ice Metrics

Sea ice can be quantified in basic terms of its concentration (SIC) and thickness (SIT). Both measures are important for scientific and marine use. SIC refers to the amount of ice cover within an arbitrary area, expressed as a percentage, decimal, or fraction. Additionally, horizontal coverage can be expressed as either sea ice extent (SIE) or total sea ice area (SIA). Total SIA is the actual horizontal area occupied by sea ice, while SIE is the area of the ocean's surface within a boundary that encompasses some minimum threshold for ice, typically taken to be a concentration of 15% (Comiso et al., n.d.; Fetterer & Knowles, 2004). This means that total SIA is a better metric than SIE for the "amount" of ice and is practically always smaller than SIE. Total SIA is easier to compute, particularly with modelled data, and as such this study will give it preference over SIE. However, SIE has been frequently used with satellite-derived data and has been the standard for communicating the amount of ice in the Arctic; therefore, some discussion will also be given to SIE. Satellite products have given preference to SIE because there is some error during melt seasons associated with distinguishing between open ocean and melt ponds, as well as a variable gap in coverage near the pole. Horizontal ice coverage is much easier to measure than is SIT and thus has been more widely used by the scientific community.

Total Arctic sea ice volume (SIV) represents the total amount of ice in the Arctic and cannot be determined without knowledge of thickness distribution. However, details of sea ice thickness, and by extension volume, are limited by sparse spatial and temporal observations.

2.2. The Community Earth System Model

To investigate ice climatology, output was used from the National Center for Atmospheric Research's (NCAR) Community Earth System Model, version 1 (CESM1) configured with the Community Atmosphere Model, version 5 (CAM5) (Hurrell et al., 2013). The sea ice component of CESM1 is the Los Alamos National Laboratory Sea Ice Code, version 4 (CICE4) (Hunke et al., 2017). CESM1 has shown to be successful at capturing sea ice trends on an annual scale, as well as trends associated with climatic changes (Stroeve et al., 2012). CESM1 features several improvements over predecessor models (such as CCSM4), notably land use and cycles of carbon and vegetation. The sea ice component also received improvements in the handling of shortwave radiation physics related to melt ponds and aerosols (Holland et al., 2011).

2.3. The Large Ensemble

The CESM1 Large Ensemble (LENS) project is a publicly available dataset of CESM1 simulations. (Kay et al., 2015). Each of the 40 ensemble members are initialized with round-off differences in air temperature (on the order of 10^{-14} K), and subsequently

receive an external forcing that is identical among ensembles. The historical portion, 1920-2005, is subjected to observed solar and atmospheric forcing as set forth by Lamarque et al. (2010). These assume well-mixed greenhouse gases and short-lived aerosols that include anthropogenic emissions, biomass burning, and volcanic activity. From 2006-2100, the high-emissions scenario, RCP8.5 is the prescribed greenhouse gas forcing (Lamarque et al., 2011; Meinshausen et al., 2011).

The slight differences in initialized temperature generates variability among the ensemble members, which varies temporally and spatially, as the result of internal climate variability. The benefit of the LENS is the large number of ensemble members, which dwarfs the size of previous ensemble projects. Both the ensemble average and the trajectory of individual ensemble members are useful for investigating climate. The ability to assess internally generated variability is another key advantage of the LENS dataset. The spread in LENS is preferable to the spread in CMIP5, which is the result of different models with different internal processes and parameterizations.

Sea ice in LENS shares a grid with the ocean and features a displaced pole over Greenland, which ensures that grid cells near the pole are not trivially small. Horizontal resolution of all components is approximately 1°, while the atmosphere consists of 30 levels. LENS output is available to the community at multiple temporal resolutions, including monthly, daily, and 6-hourly (for selected years).

Because of the climatic scales of this study, and the considerable amount of variability in ice conditions associated with weather events on daily and finer timescales, monthly resolution will be analyzed.

The LENS dataset includes a variety of variables related to sea ice, including SIT and SIC. Thickness output is given as the area averaged volume of a grid cell, i.e. the product of thickness and grid cell area is the volume of ice within that cell. Concentration output is the measure of the horizontal coverage of ice within a grid cell, ranging from 0% to 100%.

2.4. Observational Concentration/Extent Data

The Sea Ice Index, Version 3 is a long term observational dataset of ice concentration derived from passive satellite instrumentation (Fetterer et al., 2017). The full observational history ranges from October 1978 until the present. Observation platforms that have contributed to the dataset included the Nimbus-7 Scanning Multi-Channel Microwave Radiometer (SMMR), Special Sensor Microwave Imagers (SSM/I), and Special Sensor Microwave Imager/Sounders (SSMIS); the latter two are part of the Defense Meteorological Satellite Program (DMSP) (Curtis & Adams, 1987; Gloersen & Barath, 1977). From 1978 until 1987 Nimbus-7 returned SIC once every two days, which increased to daily when succeeded by DMSP satellites. Horizontal resolution is approximately 25 km. The resulting gridded ice concentration is also the primary source for determining observed total SIE and SIA

in this study. Finally, the Sea Ice Index contains a gap in coverage near the pole ("pole-hole") due to satellite orbital inclination, which has ranged in radius from 611 km in 1978 to 94 km at present.

2.5. Modelled Thickness/Volume Data

Observations of sea ice thickness are limited spatially and temporally, as well as by quality. This applies to total SIV as well, since volume can only be calculated with the inclusion of a vertical ice thickness. The best observations are those made by upward looking sonar onboard US Navy submarines, however these records are not complete spatially or temporally, and future cruise plans are not revealed as a matter of security (Kwok & Rothrock, 2009). Additionally, thickness has been derived from freeboard measurements by the ICESat and CryoSat programs (Laxon et al., 2013). In order to use a consistent and complete dataset to compare with to LENS thickness/volume, this study will utilize output from PIOMAS (Schweiger et al., 2011; Zhang & Rothrock, 2003). PIOMAS is a coupled ice-ocean model that assimilates ice concentration and sea surface temperature observations, along with atmospheric forcing from NCAR and National Center for Environmental Prediction (NCEP) reanalysis datasets. Horizontal resolution is approximately 0.8° and is available for download as monthly averages. The model has been shown to capture more than 50% of the SIT variance along submarine tracks (Schweiger et al., 2011). Because of the model's skill at accurately assessing ice conditions, and its complete record since 1979, it has been used as the best ground-truth for SIT, such as in

Zhang et al. (2013). Finally, Labe et al. (2018) found that PIOMAS could be used satisfactorily as a reanalysis dataset, and that multiple modes of real physical variability were expressed concurrently by PIOMAS and LENS.

3. Methods

3.1. Climatology Calculations

Climatologies have been calculated for SIC, SIT, and IN. Observations and PIOMAS data were used for comparison with LENS for SIC and SIT, respectively. LENS climatologies were calculated for SIC, SIT, and IN (for OW and PC6 vessels). Climatologies were calculated as a monthly average at each grid cell for the period of interest. For LENS climatologies, the ensemble average was used. The difference between LENS and the sea ice index/PIOMAS are used to show spatial bias in LENS.

Extensions of these climatologies are the time series of SIA and SIV, which are compared to the sea ice index/PIOMAS. These are shown as one-year running averages, and the difference is used to show total bias in LENS.

3.2. The Ice Numeral

The equation for Ice Numeral is:

Equation (1)

$$IN = \sum_{i=1}^{n} C_i \times IM_i$$

where C_i and IM_i are the concentration and Ice Multiplier of ice type i, respectively, for n ice types. Here, concentration ranges from 0 to 10, such that open water is zero

and 100% ice cover is 10. Ice Multiplier is an integer that is a function of a vessel's ice capability and the age and thickness of the ice. The summation accounts for the fact that multiple types of ice can occur together, in addition to open water that exists when total SIC is less than 100%. Ice multiplier ranges from -4 (thickest ice, or greater than ~1.5 meters for a vessel with no ice strengthening) to 2 (open water). This yields a range of IN from -40 (100% coverage of thickest ice) to 20 (100% coverage of open water). IM values are prescribed in a table format by AIRSS (Table 3). The Ice Numeral is designed for use by ship's transiting the Arctic, on site. A vessel's bridge watch-stander is expected to continually calculate the IN when ice conditions are perceived to change. In the Canadian Arctic, a vessel is not permitted to transit a negative IN regime, but may proceed through positive or neutral regimes (Transport Canada, 2010).

Table 3: Ice multipliers as specified by AIRSS. Types A and E refer to PC6 and OW, respectively.

CIS/WMO Ice Codes	Ice Types	Thickness	Ice Multipliers for each Ship Category						
			Type E	Type D	Type C	Type B	Type A	CAC 4	CAC 3
7• or 9•	Old/Multi-Year Ice		**-4**	-4	-4	-4	**-4**	-3	-1
8•	Second-Year Ice		**-4**	-4	-4	-4	**-3**	-2	1
6 or 4•	Thick First-Year Ice	> 120 cm	**-3**	-3	-3	-2	**-1**	1	2
1•	Medium First-Year Ice	70-120 cm	**-2**	-2	-2	-1	**1**	2	2
7	Thin First-Year Ice	30-70 cm	**-1**	-1	-1	1	**2**	2	2
9	Thin First-Year Ice - 2nd stage	50-70 cm							
8	Thin First-Year Ice - 1st stage	30-50 cm	**-1**	-1	1	1	**2**	2	2
3 or 5	Grey-White Ice	15-30 cm	**-1**	1	1	1	**2**	2	2
4	Grey Ice	10-15 cm	**1**	2	2	2	**2**	2	2
2	Nilas, Ice Rind	< 10 cm	**2**	2	2	2	**2**	2	2
1	New Ice	< 10 cm	"	"	"	"	"	"	"
	Brash (Ice fragments < 2 m across)		"	"	"	"	"	"	"
=Δ	Bergy Water		"	"	"	"	"	"	"
| | | |	Open Water		"	"	"	"	"	"	"

A team from the National Research Council of Canada investigated a sample of ship transits, corresponding INs, and whether or not ice damage was sustained (Timco & Kubat, 2001). They determined that the system performed "reasonably well," although damage was also shown to be correlated to vessel speed, which is not included in the IN calculation.

Note that Table 3 differentiates vessels by a "Ship Category" that is utilized in Canada. This study will utilize the International Maritime Organization's (IMO) Polar Class system, namely PC6 and OW vessels, which correspond to Type A and Type E, respectively (Smith & Stephenson, 2013). Whereas Table 3 has values dependent on ice age, this study will make IM entirely a function of SIT, using the method of Smith and Stephenson (2013). While IN takes into account the different ice types that exist within a given visible area, we will assume that inside a grid cell there is only one type of ice, with the possibility of open water. The average SIT for a grid cell will be used with the SIC of that grid cell, and the remaining area of each grid cell will be taken as open water. Although the model includes sub-grid-scale SIT, the output is only available as the grid average. The equation for IN is now altered so that it may be calculated with one value for each grid cell in time, space, and ensembles, as follows:

Equation (2)

$$IN = C_{grid} \times IM_{SIT} + (10 - C_{grid}) \times IM_{OW}$$

where the first term represents the ice component and the second term represents the open water component. Because the IM for open water is always 2, regardless of vessel type, the equation becomes:

Equation (3)

$$IN = C_{grid} \times IM_{SIT} + 20 - 2 \times C_{grid}$$

3.3. Determination of Interannual Variability

In this study interannual variability was derived for all relevant ice metrics from time series of the LENS output from 1920-2100. These are completed using either an Arctic average (for SIC and SIT) or total values (for SIV and SIA). Determining this variability among sea ice metrics is challenging due to the strong signal of climate change. To avoid spurious interannual variability in the data arising from a strong trend, the difference between one year and the next is calculated for each month. In this way, if an interval of rapid ice loss (or gain) resulted in a large but constant annual change, the interval would be represented by a constant year-to-year difference and therefore no interannual variability. From this annual difference time series, a three-year running standard deviation was performed, which is the variability that will be interpreted in this study. The three-year running standard deviation is a representation of four years of raw sea ice data. The use of three years in the standard deviation was somewhat arbitrary, as utilizing different windows produced very similar results, albeit larger windows produced smoother curves. The resulting variability curves can be used for identifying peak variability, as well as its timing and amplitude.

To verify that any variability changes detected in the analysis were not the result of the trend in the data, the analysis was repeated with the use of Gaussian white noise

(GWN). The ensemble average sea ice trend was combined with a GWN signal, which created a data-set with a strong trend as well as random input. The original analysis was then repeated on 10,000 random generations of the trended GWN signal.

Comparison of variability curves of different ice metrics was accomplished by normalizing them for each month. For each month, the time series mean was subtracted and then divided by the time series standard deviation. The end result is a dimensionless variability curve for each metric that can be compared to other metrics for the same month. This is useful for identifying the timing of peak variability amongst the several metrics.

4. Results

4.1. Model Performance

4.1.1. Model Climatology

A climatology of simulated sea ice conditions is presented in Figures 2 and 3 for SIC, and Figures 4 and 5 for SIT. These climatologies are 40-year ensemble averages, and they represent "typical" ice conditions present during different periods. These climatologies also help display the patterns of sea ice retreat over time. Notably, the decrease in ice extent occurs earlier in summer than in winter. Additionally, in the summer, the ice largely retreats from the Eurasian coast and central Arctic basin towards the Canadian archipelago. For much of the 21st century, winter SIA only sees meager declines near the marginal ice zones. SIT shows a visible decline in all months, with summer transitioning to ice-free conditions in mid-century. The winter months show SIT declining at all spatial points, but never reaching ice-free conditions within the LENS run.

Limited IN climatologies are also presented in Figure 6. These represent only the months of September (annual minimum ice extent) and March (annual maximum), for the period of 1960-1999. IN can range from -40 (worst conditions) to 20 (open water). These climatologies illustrate the typical "go/no-go" (navigation permitted/not permitted) zones for the two vessel types considered in this study. In March, the entire Arctic was highly inaccessible (ensemble average close to -40). In September, the accessible areas were greatly expanded, however the climatology

still indicates that all shipping routes were inaccessible through the 20th century on average, even with a moderately ice-strengthened ship.

4.1.2. Area/Concentration Bias

To evaluate the CESM sea ice simulation, beyond that shown by Stroeve et al. (2012) and Hurrell et al. (2013), the model's output was compared against other sources. Figure 7 shows 12-month running means of SIE for each ensemble and the satellite-derived Sea Ice Index. Boxplots illustrate the ensemble spread of the bias of each calendar year. The model consistently produces a greater amount of ice than observed. Early in the record, the median ensemble bias is less than 5% of the observational value (both positive and negative), but a general trend can be discerned of rising positive bias throughout the observational record. This implies that the model is not fully representing the recent loss of sea ice. Several CMIP5 have been shown to have a similar, or worse, bias (Stroeve et al., 2012).

SIA displayed in two-dimensional space becomes SIC (an arbitrary horizontal area occupied by some area of ice). The spatial structure to this bias is displayed in Figures 8 (late 20th century) and 9 (Early 21st century) as the difference in SIC (LENS minus observations). In the interior of the Arctic, LENS has little bias during the winter months, but tends to overestimate ice in the summer. Year round, there is an overestimation of ice in the marginal ice zones, and in the winter in the Sea of Okhotsk. In the later period (Figure 9), the overestimation of the marginal ice zones

(particularly in the Atlantic region) increases, which corresponds to the increasing positive bias of SIA in Figure 7.

4.1.3. Volume/Thickness Bias

Figure 10 displays the comparison of LENS total SIV to PIOMAS, as 12-month running means. As with SIA, LENS tends to overestimate the ice volume given by PIOMAS, but there is no noticeable temporal trend in the bias of SIV. However, the downward trend in volume means that the relative bias, as a percentage of the volume, is increasing, rising from ~28% to ~50% of the PIOMAS volume.

When SIV is considered spatially, it becomes SIT (volume divided by an area). As with the bias in ice volume, the spatial bias of SIT is very consistent month-to-month and between the early (Figure 11) and late record (Figure 12). Here, the source of the greatest thickness bias in LENS becomes apparent: ice trapped within the Canadian Archipelago, which in LENS, reaches a maximum thickness of 63.4 meters and a maximum age of 478 years, which are physically unrealistic. However, this extremely thick ice regionally does not dominate total SIV across the basin. Table 4 shows the minimal effect on Arctic SIV when grid cells are capped at specific values of thickness. Figures 11 and 12 are shown with a 5-meter maximum thickness to better illustrate the rest of the Arctic, however the saturated red areas often greatly exceed 5 meters in bias. It has been shown, however, that PIOMAS underestimates

total SIV, particularly thickness in the Canadian archipelago and near the Greenland coast (Labe et al., 2018).

Table 4: The effect on LENS averaged total Arctic SIV, when a thickness cap is placed on all gridcells.

	Thickness Capped at (m):			
	No Cap	40	20	10
Mean SIV (1000 km^3)	2.13	2.11	2.06	1.98
Percent Change		**1%**	**3%**	**7%**
Max SIV (1000 km^3)	4.97	4.93	4.81	4.65
Percent Change		**1%**	**3%**	**6%**

4.2. Variability of Sea Ice Metrics

Figure 13 displays a simple approach to viewing sea ice variability and offers some motivation for further investigation. The checkerboard plot shows the time-series anomaly (September only) of each of the 40 ensemble members of total SIA. Even at first glance, it is apparent that there is an interval of high variability in the early to mid-20^{th} century. The period in the vicinity of peak ice-loss in the ensemble-mean, near 2020, appears to have very high variability, which has been displayed in greater detail in the lower plot. Finally, there is little variability late in the LENS run, as SIA approaches zero. The checkerboard plot is also useful for viewing the ensemble variability, which can be seen easily by comparing ensemble members 15 (positive anomalies begin in 2018) and 13 (negative anomalies persist until 2026) for example.

Figures 14-17 represent the year-to-year difference and corresponding derived variability for four ice metrics. The thin blue curve represents the actual year-to-year change, and the thick blue line is the five-year running change. In SIA (Figure 14), several features become apparent: variability in SIA has a shape that repeats in most months; variability peaks at different times in different months; and variability peaks coincide with peak ice loss. In every month, there is an increase in SIA variability in the future. The typical shape (as exemplified by November) of the variability curve consists of five stages:

1.) fairly constant baseline variability before the onset of anthropogenic ice loss
2.) a gradual rise in variability
3.) a peak that coincides with peak rate of ice loss
4.) a steeper downward slope of decreasing variability
5.) little-to-no variability associated with an ice-free Arctic ocean in that month

September, the annual ice minimum, experiences this peak variability first, occurring around 2030. At the other extreme are the late winter/early spring months, which display only modest rises at the end of the century. This suggests that the characteristic evolution exhibited by warmer months might occur in the winter as well, but past the end of the LENS run. Here, it is important to reinforce that the variability expressed here is not an artifact of the ice loss trend; the effect of taking the year-to-year difference removes the effect of a large but constant change

during a rapid-loss interval. This was additionally verified by repeating the analysis 10,000 times on a trended GWN signal, which resulted in no peaks in variability.

Figure 15 displays the same curves for year-to-year difference and associated variability in total SIV. Interestingly, SIV shows a much different response than SIA. Unlike the five stages of SIA variability listed above, SIV variability exhibits a pattern with a broad peak that is smaller in amplitude.

The absence of a pronounced peak in SIV variability is the first large contrast that can be drawn between the two metric's variability curves. Secondly, there is a difference in timing. Peak variability occurs earlier in SIV than in SIA in all months except April (December being a prime example). The year-to-year differences (blue curves), of both SIA and SIV, display several pronounced but short-term increases in sea ice during the 20th century. These correspond to volcanic eruptions (notably Mount Pinatubo in 1991) and has been described in Gagne et al. (2017). There is a noticeable step-like change in the year-to-year difference of SIV in the early 1990s that is mainly resultant from the Pinatubo eruption, which acts to interrupt the beginning of significant ice-decline and resumes promptly following the conclusion of the volcanic forcing.

Figure 16 is the corresponding variability of the Arctic-averaged change in Ice Numeral for open-water vessels, IN_OW. Its shape is very similar to the five stages of

SIA variability identified above. However, some key differences from SIA can be discerned:

1.) peak variability is much broader
2.) timing of the peak is shifted earlier (~6 years)

These are the first indications that, like IN itself, IN variability is shaped by both SIC and SIT. By comparison, the peak variability of IN_PC6 occurs earlier time than for an open-water vessel and the peak is become broader (Figure 17). This mismatch in timing resembles that of the mismatch between SIA and SIV and indicates that IN_OW is more sensitive to SIC, while IN_PC6 is more sensitive to SIT. On the variability spectrum, bounded by the peaks exhibited by SIA to SIV, the IN variabilities generally sit in between with regard to both timing and shape. As shown in Figure 18, in almost every month the normalized variability curves of all four metrics show the same progression of peaking variabilities from earliest to latest: SIV, IN_PC6, IN_OW, and SIA.

The timing of the peaks is also depicted in Figure 19. Here each peak is shown as a point for each month and metric, alongside the median year of peak variability among all ensemble members for each metric. With the exception of only two months (April and July), the variability peaks (or occurs simultaneously) in the same order. April appears as a large outlier for SIA, but with reference to Figure 14, it can

be seen that variability is largely constant for the entire LENS run, and thus the century-ending increase in variability is small in amplitude before being truncated.

4.3. Spatial Patterns of Peak Variability

The variability previously expressed has represented the entire Arctic. Spatially, however, variability peaks are not homogenous. Figure 20 shows the magnitude and timing of variability peaks of SIC for each grid cell, as well as the time of peak ice loss rate. SIC variability peaks generally coincide with peak ice loss, and the spatial patterns in Figure 20 reflect this. Variability during March does not contain distinct peaks in the interior, though, as peak ice loss occurrence is truncated by the end of the LENS run (bottom row of Figure 20). The middle row of Figure 20 depicts the year that maximum variability occurs, which clearly is early for September and late for March (consistent with Figure 14).

Contrasting SIC, the peaks of SIT variability are largely homogenous spatially, which is consistent with the broad peaks in the time series of Figure 15. In amplitude (top row, Figure 21), the months of March and September are nearly spatially uniform and similar to each other, with small peaks in the Canadian archipelago. The timing of peak SIT variability (middle row, Figure 21) displays some small differences between March and September. In March, the coastal areas peak much closer to the end of the century, while the interior of both months peaks early in the century. This is consistent with March peaking later than September in Figure 15.

The corresponding patterns of IN are displayed in Figure 22 for OW and Figure 23 for PC6. As previously seen in Figure 18, IN variability takes contributions from both SIT and SIC and exists on a spectrum in between; IN_PC6 falls closer to SIT and IN_OW falls closer to SIC. The bottom rows of Figures 22 and 23 show that IN maximizes earlier for a PC6 vessel in both months (more evident in March). IN_OW, whose variability is closer to SIC's, shows greater amplitudes near the Atlantic and Pacific boundaries in March, and in the interior during September; this closely resembles the pattern displayed by SIC in Figure 20. In contrast, this effect for IN_PC6 seems to be dampened and a more homogenous pattern is seen in Figure 23, resembling the pattern displayed by SIT.

4.4. Ice Numeral Behavior

It has been previously shown that IN variability contains a blend of the variability of SIA and SIV. This makes sense, as the IN equation is a function of SIC and SIT. It is interesting that for a PC6 vessel, IN variability relates more closely with SIV than SIA (and vice versa for OW). It is obvious that IN relates to its components, however, it is not obvious which component is more important for each vessel class, different temporal scales, and spatial points.

Figure 24 shows correlation maps for IN_OW and its components for the months of March and September. Ice components and IN are anti-correlated, as increasing ice

cover results in a decreased IN (negative INs relate to unfavorable shipping conditions). The correlation maps represent the historical portion of the LENS run, 1920-2005 (i.e. before the most significant ice loss period). For SIC, in the month of March (top left of Figure 24), there are three generalized regimes:

1.) The central basin with perfect anti-correlation
2.) The fringe-areas within the Arctic Ocean with modest to almost no correlation
3.) The marginal ice zones outside the Arctic basin with perfect anti-correlation.

In September (top right of Figure 24), the low correlation areas strengthen and shrink to a central area near the pole.

For IN_OW correlation with SIT (bottom row of Figure 24), a very different regime pattern is displayed:

1.) The interior Arctic basin with moderate to almost no correlation
2.) The marginal ice zones with perfect anti-correlation.

IN_OW and SIT correlation patterns are broadly similar between March and September, however, the marginal ice zone and perfect anti-correlation areas retreat and compact northward in September.

Figure 25 shows the same four plots, but for a PC6 vessel. The major difference is that the areas of high correlation between IN and SIC have shrunk.

Table 5: Geographic location of points used in Figures 26-29. They are also annotated for reference on Figure 24.

Point	Latitude	Longitude	Note
1	86°N	90°W	North of Ellesmere Island, Canada
2	85°N	90°E	North of Severnaya Zemlya, Russia
3	75°N	45°E	Barents Sea

To help interpret the patterns displayed in Figures 24 and 25, the relationship between IN and its components for three different grid cells are shown in Figures 26-29. These particular sites were chosen to represent regions showing starkly different relationships. Table 5 lists the locations and descriptions of all three selected points, which have also been illustrated on Figure 24. At Point 1, IN_OW is perfectly anti-correlated with SIC, but has a very weak correlation with SIT (Figure 26). Because the equation for IN places SIT into bins, a certain range of thickness is needed to generate a change in ice multiplier. At Point 1, in the interior of the ice pack, SIC in March is always 100% and SIT does not fall below the threshold to generate a lower IM, therefore IN is dictated by SIC. Point 2 is similar, except that SIT occasionally ranges to values that are thin enough to generate changes in IM (and therefore IN). This creates a weak correlation with both components. Finally, Point 3 displays an interesting relationship, because at this point on the sea ice

margin there is a full range of SICs, and multiple IMs (evident by the discontinuities in the lower left plot of Figure 26). The upper left plot of Figure 26 shows several linear patterns that the scatter plot has been organized into. Each line corresponds to a range of SICs when the IM is constrained by a limited range of SIT.

These linear elements can be expressed by rearranging equation (3):

Equation (4)

$$IN = 20 + (IM - 2) \times C$$

When the range of SIT is sufficiently small as to not change the IM, then IN is a simple linear function of SIC, with the slope represented by *IM-2*.

The right columns of Figures 26-29 represent the ensemble averages of the corresponding left-column plots, which results in one point per year at each of the three selected sites. The primary effect of ensemble averaging is to remove the most extreme ensemble occurrences. In this manner, the discrete regimes displayed by the individual ensembles are removed, leading to generally stronger linear relationships. This is a simpler way to view the relationship between IN and its components, as the data are not forced into discrete regimes. Viewing the relationship of IN and its components demonstrates the drivers of IN.

When comparing IN_OW (Figures 26 and 27) to IN_PC6 (Figures 28 and 29), the first obvious difference is that IN_PC6 is consistently shifted to higher IN values,

reflecting the benefit of an ice-strengthened vessel. Additionally, correlation coefficients are weaker between IN and SIC for a PC6 vessel than for an OW vessel, and the opposite is true for the correlation between IN and SIT. This reinforces the finding that IN_PC6 is more dependent on ice thickness and IN_OW is more dependent on ice concentration.

For almost all instances, regardless of vessel or metric, September (Figures 27 and 29) displayed stronger correlations than March (Figures 26 and 28). This was true for the ensemble average and for individual ensembles. This is due to the increased spread in September, whereas March is more closely bounded to upper limits of both SIC and SIT.

The relative importance of each component can be seen in Figure 30, which displays the ratio of the correlation coefficient of IN vs. SIT to the correlation coefficient of IN vs. SIC, with all ensembles included. Because this figure shows the *relative* strength of each correlation to each other, it does not indicate absolute strength of the correlations, which are displayed in Figures 24 and 25. Blue areas indicate that the correlation of IN vs. SIC outweighs the correlation of IN vs. SIT, and red represents the opposite. SIC dominates a large portion of the interior in both March and September, and for both vessel types, reflective of the linear structures expressed by equation (4). SIT plays a much larger role in the month of March than in September, reflecting the smaller range of ice multipliers present in March. September is

characterized by SIC dominance in the interior, and similar correlations at the marginal ice zones. The consistent presence of blue areas in the interior are reflective of thick ice that results in IN that can only vary with a change in SIC. Because these marginal zones in September usually have thin or no ice, the change between the presence and absence of ice creates a similarly high correlation for both components. Finally, in both months SIT plays a larger role for a PC6 vessel than for an OW vessel.

5. Discussion

Implications for Predictability

The interannual variability of Arctic sea ice is expected to increase in the future. While the amplitude and timing varied among metrics, the increase in variability is a robust feature of the CESM under RCP8.5, as well as CMIP5 models (Mioduszewski et al., 2018). This is important, as the trend in all relevant sea ice metrics is for increasing potential of shipping traffic, yet the rise in variability hinders reliability of sea routes. This finding is in contrast to the picture of quickly expanding marine polar traffic (Pizzolato et al., 2016; Smith & Stephenson, 2013). The increases in interannual variability are not directly comparable to operational timescales, however, the importance of predictability on operational timescales, such as weekly to seasonal, cannot be understated as shipping success the previous shipping season means little for operational strategy. Seasonal and 30-day outlooks of SIC and SIT are available through services such as the US National Ice Center and the Canadian Ice Service, though products are limited during the winter. Additionally, IN is not forecasted by these services and mariners must interpret with their own judgement how SIC and SIT forecasts will affect their transit. Current sea ice predictability varies depending on the forecasted metric, whether it is regional or pan-Arctic, and the month of initialization. For most cases, predictability on the order of weeks to seasons are reasonable (Guemas et al., 2016). The analysis of IN completed here demonstrated how choice in vessel affected the sensitivity between SIC and SIT, which in turn means that predictability of different metrics have a different

importance for different vessels. Guemas et al. (2016) showed that SIT and SIV are more predictable than SIA and SIC, which, for a less capable vessel that is more susceptible to ice concentration (such as OW vessels), could lead to mishaps. The actual time taken to transit the Arctic is relevant to predictability as well. NSR transits averaged near 20 days in the 1990's and were reduced to 11 days in 2012-2013 (Aksenov et al., 2017). TSR and NWP transit times can be expected to exceed those numbers, which puts the actual transit duration near the limit of sub-seasonal predictability (Bitz & Stroeve, 2014).

From the LENS output, an example of the impact of variability produced by ensemble members can be seen in Figure 31. The large plot is the ensemble and decadal average of IN_OW in September for the period of 2016 to 2025. This map shows typically favorable conditions for shipping along the NSR during this decade. However, the smaller plots show the variability simulated by a particular ensemble member from year-to-year. When not expressed as an ensemble average, it can be seen that there is a great deal of interannual variability, and the NSR repeatedly opens and closes during the decade; 2016, 2018, 2019, 2022, 2023, and 2025 are favorable for shipping while 2017, 2020, 2021, and 2024 are unfavorable.

Features of the Ice Numeral

IN provides an interesting area for research, because it seems to be extremely simple, yet as the summed combination of two multiplied terms, the results of IN are

deceptively complex. Figures 26-29 provided a good demonstration of IN behavior, particularly its nonlinearity. Because SIC and SIT have behaviors that sometimes act independently, the IN acts with its own unique behavior. This is compounded by the fact that SIT is placed into discrete bins required by IM. Although it might often be preferred to assess such a function with continuous SIT data, the binning mirrors the actual way that IN is calculated on site by vessels. A modified IN formula that was altered to remove the binning could have been employed, however this study maintained the original in order to keep the results as close to a real vessel's determination as possible. Perhaps the most noticeable artifact of the binning of IM can be seen in Figure 24, where the correlation between IN and SIC have step-like changes. The binning, however, is somewhat mitigated when IN is based on ensemble averages.

Limitations of Study Methodology

The correct method for calculating IN on site involves accounting for ice of all IMs present. However, the LENS output limited this full calculation, as sub-grid scale ice thickness is not available, which forced the approximation of one ice type and/or open water in each grid cell. Mean ice thickness is a good approximation for ice in a grid cell, but several nuances may have been lost without taking into account the full range of ice. Furthermore IN may be altered by observers on vessels to account for decaying (increase to IN) or ridging ice (decrease to IN) within their field of view

(Transport Canada, 2010). These were also not accounted for by the methodology in this study, other than indirectly through average grid ice thickness.

Other limitations in this study stem from the dependence on the LENS dataset, with no reference to other models or other forcing scenarios besides RCP8.5. As previously seen, the CESM performs well at representing sea ice, but an investigation with other models may have provided additional insight. We note, however, that Mioduszewski et al. (2018) documented a similar future increase in Arctic sea ice variability averaged among CMIP5 models, including the month-to-month differences in variability characteristics simulated in LENS. Previous studies have also utilized CMIP5 simulations to predict shipping potential, without the detailed analysis of interannual variability (Melia et al., 2016; Smith & Stephenson, 2013; Stephenson & Smith, 2015). Although other emission scenarios were not analyzed, the observational record of sea ice has shown that ice cover is decreasing faster than in the LENS dataset and in other GCMs (Stroeve et al., 2012). This indicates that, for at least the short term, a lesser emissions scenario than the high-end RCP8.5 may not have been relevant.

Finally, the CESM and its LENS dataset are not without bias, as previously shown in the observational comparisons. Although these biases were marginal on most regional scales, the integrated pan-Arctic bias for SIE has grown in recent years, and the bias for SIV is a significant percentage of the modelled ice quantity. The effect

that these biases play on the results is unknown, however overestimations of SIC and SIT indicate that IN is likely to be higher in reality. A reasonable extension of this would indicate that the accurate physics of the CESM, in combination with its overestimations, mean that variability peaks occur earlier in reality. Calculations of IN from Sea Ice Index and PIOMAS data might help quantify the LENS error, or through a record of in situ IN determinations.

Difficulties of Arctic Shipping

While this study presents increases to sea ice variability as a possible impediment to Arctic shipping prospects, the Arctic ice pack is still declining, and will eventually reach ice-free summer conditions. However, there are several other factors besides growing variability that make Arctic shipping difficult. Large commercial vessels can draft (depth below waterline) a significant amount, so accurate bathymetric surveys for nautical charts are a necessity. Meager historical maritime traffic and ice conditions in the past have kept Arctic surveying to maritime standards limited. In fact, only 1% of Canadian Arctic waters are surveyed to modern standards; this number rises to 3% for marine corridors (Fisheries and Oceans Canada, 2017).

Furthermore, the Arctic is notably devoid of infrastructure and logistical support, which for a trans-Arctic transit may be tolerable, but presents issues for vessels travelling to destinations within the Arctic. Even for trans-Arctic shipping, emergencies or casualties to vessels or crewmembers may quickly turn dire without

adequate support in the region. The Arctic is a remote environment, and an increase in shipping may result in more and more ships that are on their own.

The loss of sea ice also presents the alternative challenges of open water. Wave activity increases without the dampening influence of ice, and air temperatures below freezing result in sea spray that freezes to a vessel's topside. Vessel icing is hazardous to vessel stability as well as crewmembers on deck. Moore (2012) found that in winter, in the subpolar Atlantic, ice accumulation rates of 4 cm $hour^{-1}$ are common. Taking the density of ice to be ~900 kg m^{-3}, this is equivalent to ~36 kg m^{-2} $hour^{-1}$ (Pustogvar & Kulyakhtin, 2016).

In the winter, the Arctic presents the additional challenge of extended darkness. Should shipping extend past summer months in the future, increased darkness will present difficulties in ice navigation. Even modest ice navigation can be dangerous and unpredictable, so the loss of light to aid in recognition of ice features adds to the difficulties.

Finally, it is possible that shipping may come to depend on icebreaker escorts, much as is the standard on the Great Lakes or Canada's Atlantic ports. Individual nations, or private companies, would be free to charge for ice escort services. If these fees are substantial, they could offset the gains associated with the shortened sailing distances.

6. Conclusions

In this study we have utilized the output of 40 realizations of Earth's climate from a fully coupled GCM to analyze changes to Arctic sea ice interannual variability, especially its impact to commercial shipping. From this we have determined the following key-results:

1. Sea ice variability peaks in the future

This study analyzed four sea ice metrics: total sea ice area (SIA), total sea ice volume (SIV), and ice numeral (IN) for two vessel types: open water (OW) and polar class 6 (PC6). We have shown that for all four metrics, variability experiences an increase that corresponds with ice loss from anthropogenic climate change. This increase in variability is not an artifact of the strong downward trend in sea ice area, but rather a unique feature that occurs simultaneously with the decline in ice cover.

2. Each metric's variability curve has a characteristic shape

Regardless of month chosen, variability of a given sea ice metric displayed a peak that corresponded with the peak rate of ice loss. The differences among months for a given metric primarily affected the timing of the peak. Typical SIA variability consisted of a baseline natural variability, a large rise in future variability, and finally a decrease to zero with the loss of the ice pack. SIV variability was similar, but with a variability peak that was broader and smaller in amplitude and occurred earlier in the future in each month. The peaks of IN_OW and IN_PC6 variability

occurred between those of SIV and SIA, with IN_OW acting more like SIA and IN_PC6 acting more like SIV.

3. Timing of peak variability depends on season and metric

The timing of peak variability was a function of the season. The earliest occurrences of peak variability were in the late summer/early fall (August, September, October), around 2030 for SIA. The latest occurrences of peak variability were the late winter (February, March, April), after 2090 for SIA. The early and late timing of peak variability corresponds to the timing of the annual minimum and maximum of sea ice, respectively. This is likely related to the thermodynamics of the system, as thicker and more expansive ice is limited in growth potential. Finally, the chronological peaks of variability for each metric typically occurred in this order:

1. SIV
2. IN_PC6
3. IN_OW
4. SIA

4. Vessel selection influences which IN component is more important

Vessels with lesser degrees of ice ability (such as OW) are more susceptible to the existence of any ice, which occurs first as a significant concentration with minimal thickness. As the vessel becomes more ice-capable, SIT becomes more important. We have shown that IN_OW is therefore more closely correlated to SIA, and IN_PC6 is more closely correlated to SIV.

This study comprehensively investigated the relationship of IN within the LENS output. In the future, ground-truthing of IN (and its variability) should be conducted with a combination of on-site and remote observations. The creation of reliable IN products (such as operational forecasts or analysis) that are synthesized through any available observations would be of immense value to the maritime community. Additionally, a modified IN formula could be devised that removed the discrete jumps, but preserved the relationship between IN and its components.

Figures

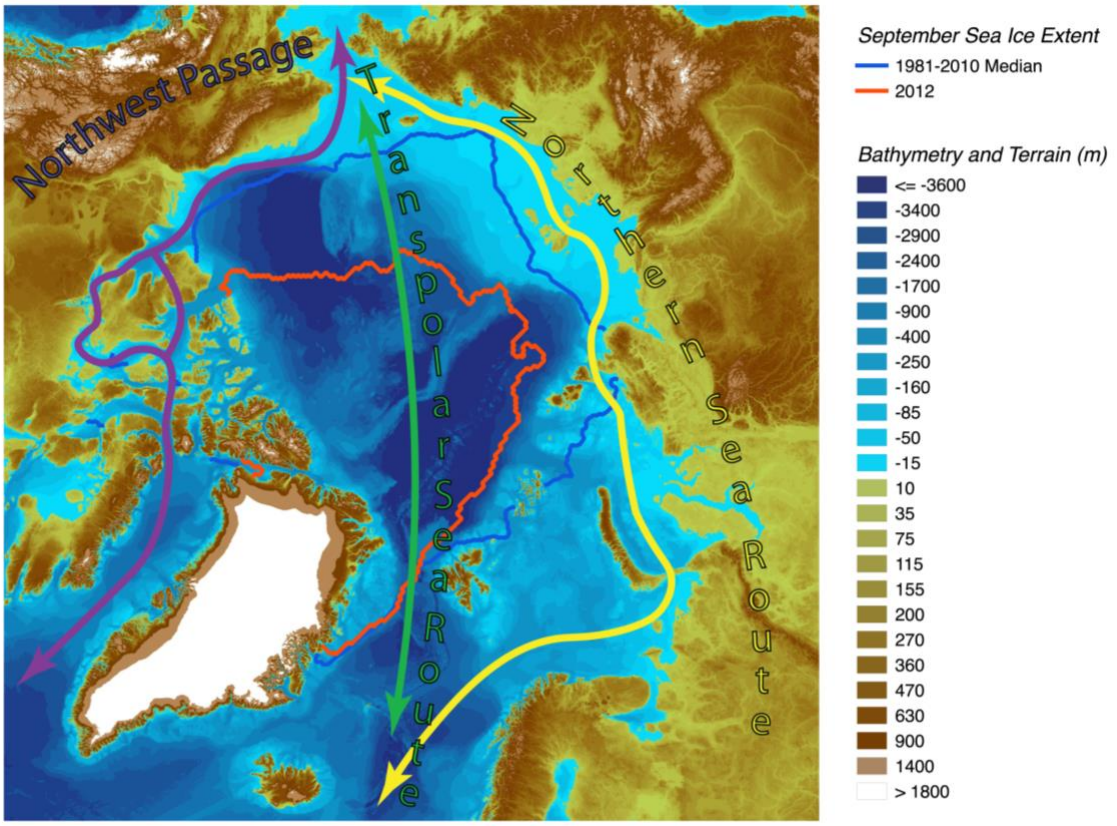

Figure 1: Thematic map of Arctic environment. The three sea routes displayed are simplified and approximated for reference. These three routes are the Northwest Passage (NWP) in purple, the Northern Sea Route (NSR) in yellow, and the Transpolar Sea Route (TSR) in green. Also shown is bathymetry (see legend) and September sea ice extents (SIE) for the 1981-2010 median (blue) and 2012 (the record minimum, green). Bathymetric data is taken from the International Bathymetric Chart of the Arctic Ocean (IBCAO) and sea ice extents are taken from the Sea Ice Index (Fetterer et al., 2017; Jakobsson et al., 2012).

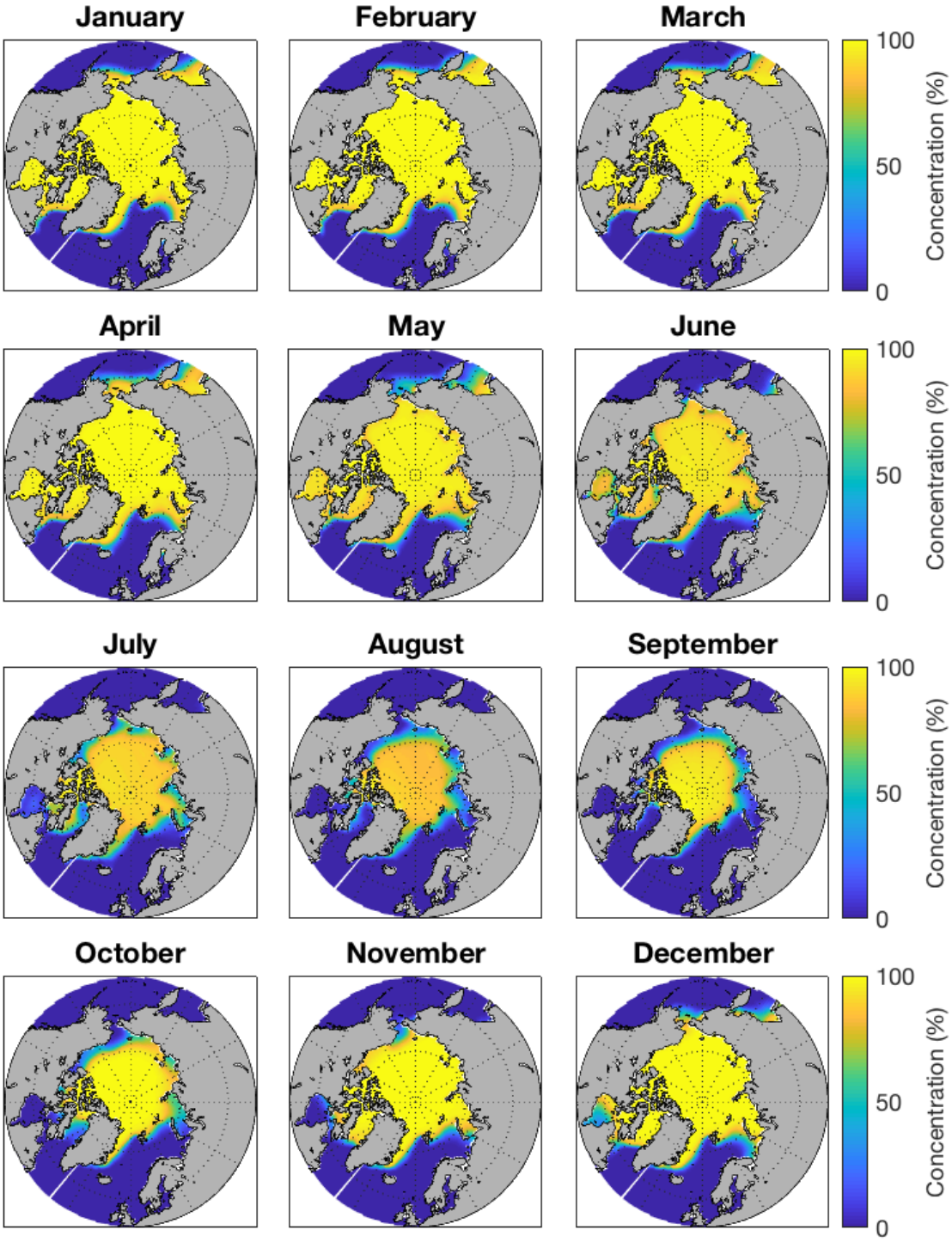

Figure 2: LENS ensemble averaged SIC climatology. 1920-1959.

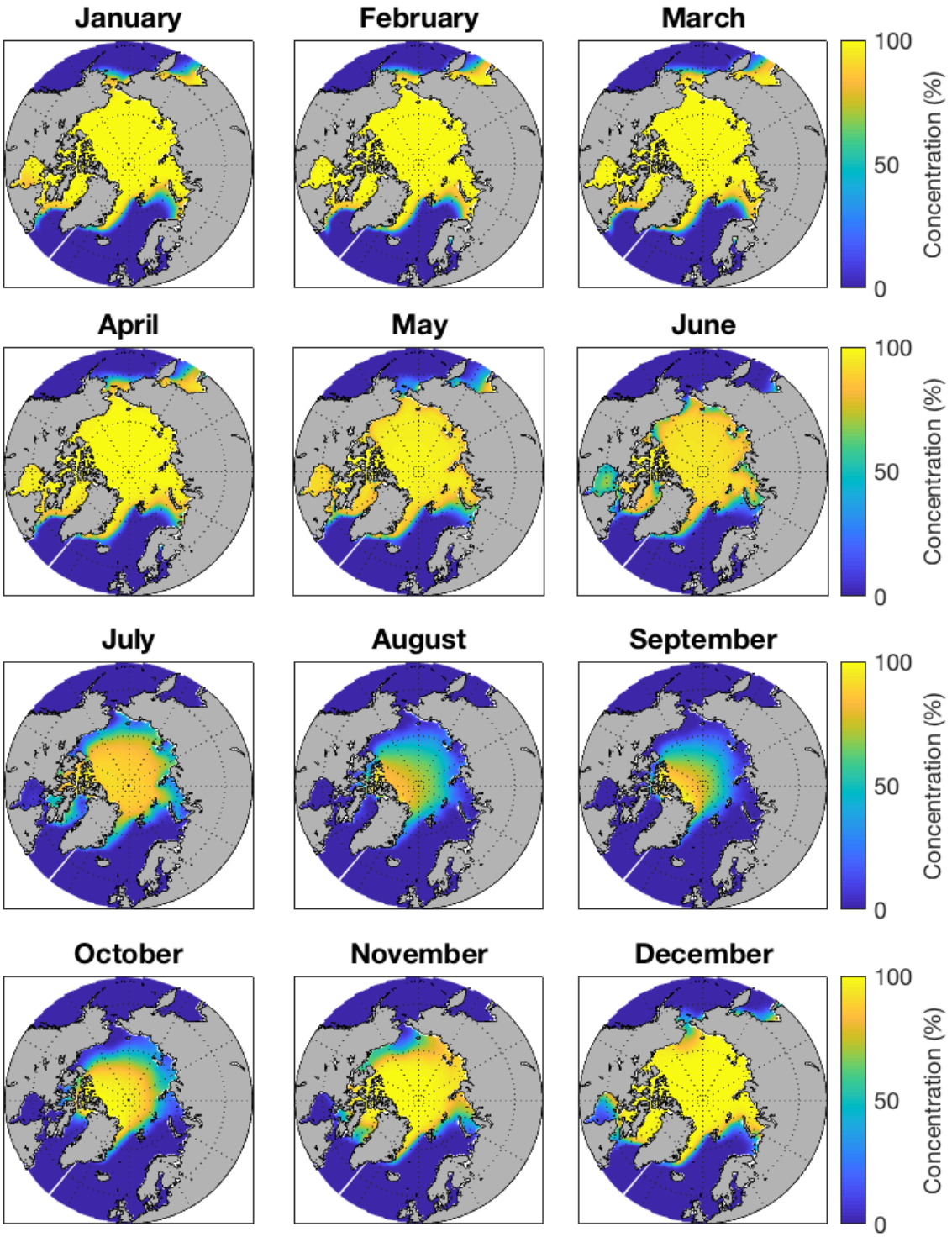

Figure 3: LENS ensemble averaged SIC climatology. 2000-2039.

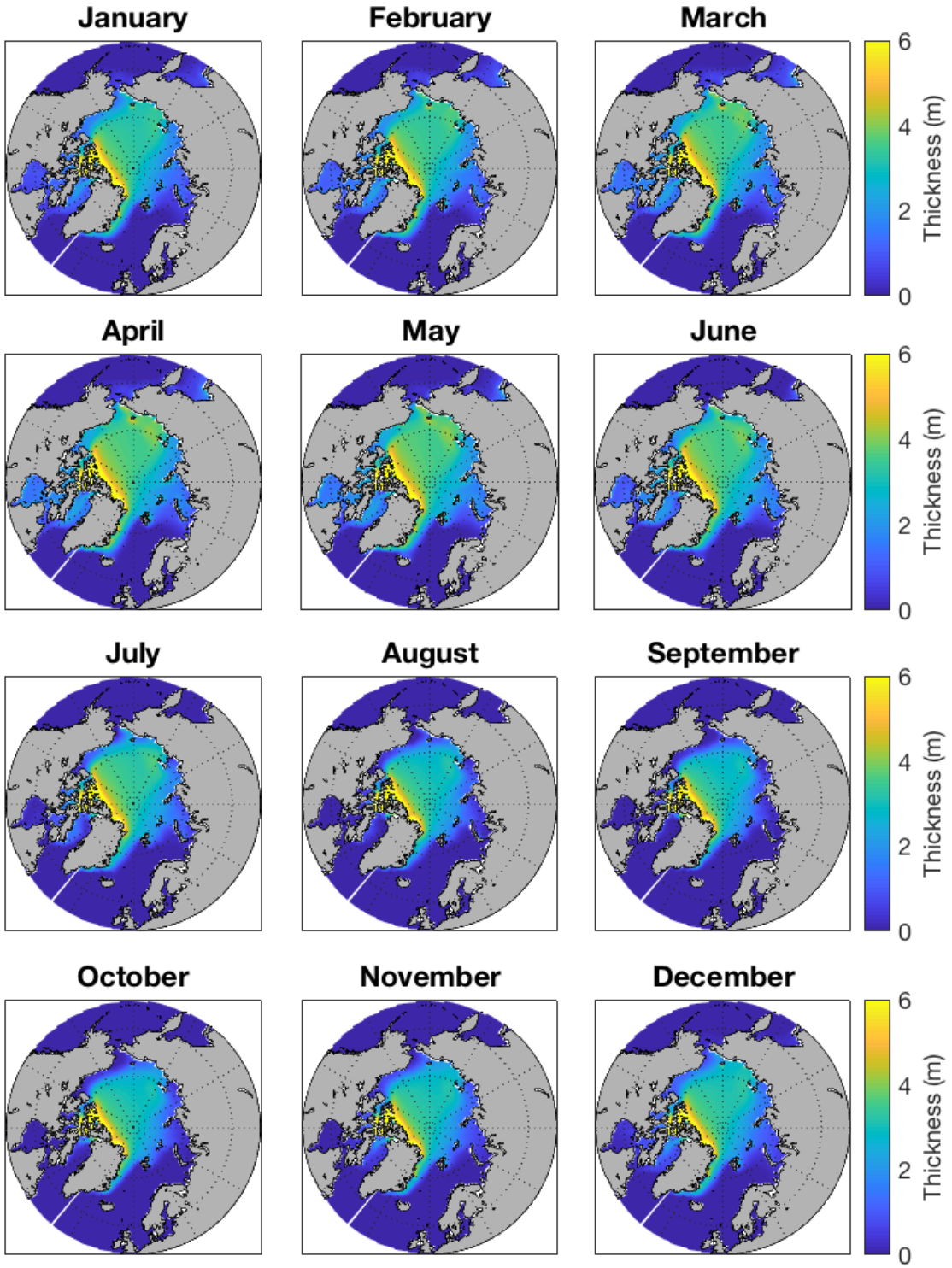

Figure 4: LENS ensemble averaged SIT climatology. 1920-1959.

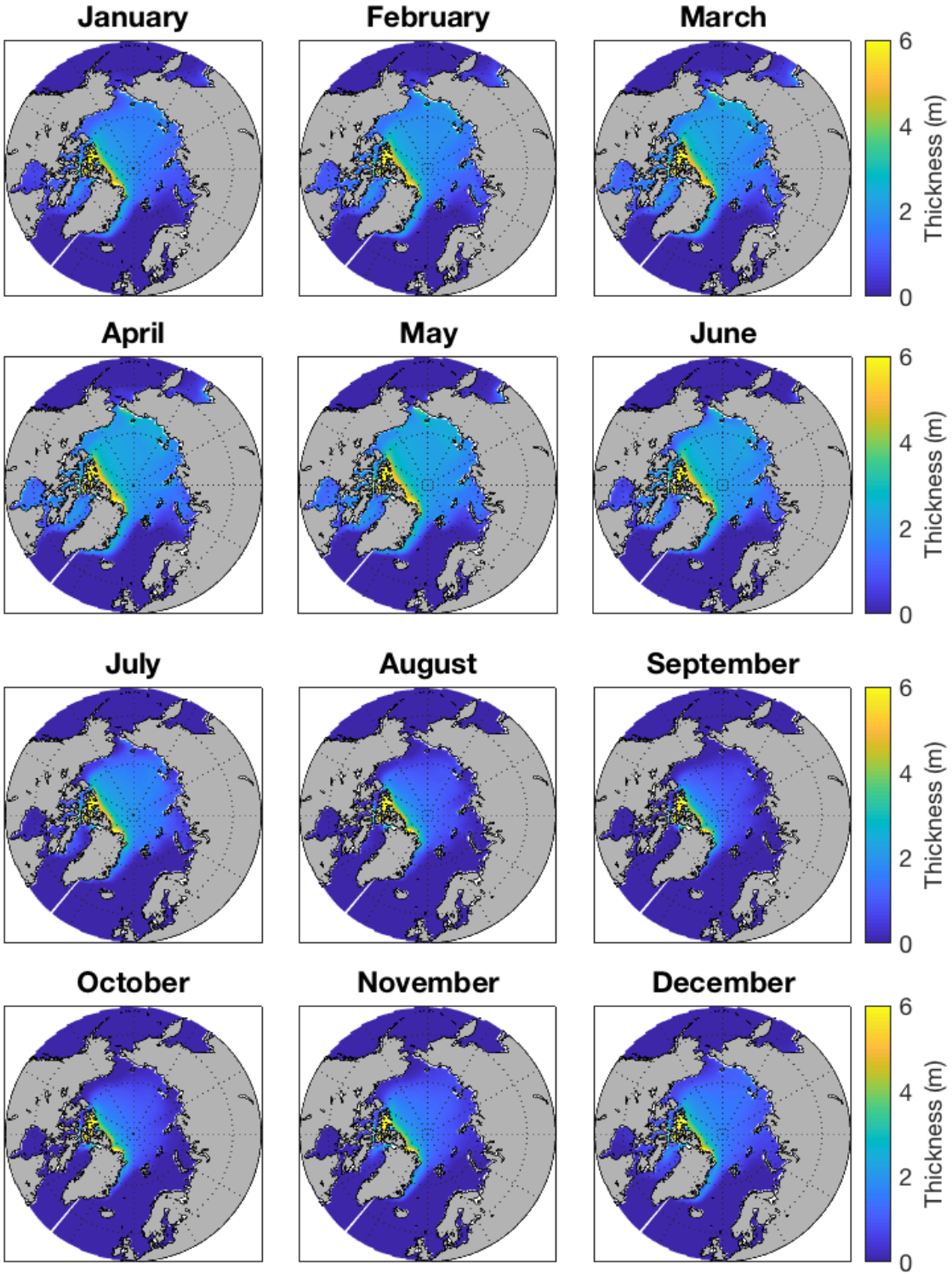

Figure 5: LENS ensemble averaged SIT climatology. 2000-2039.

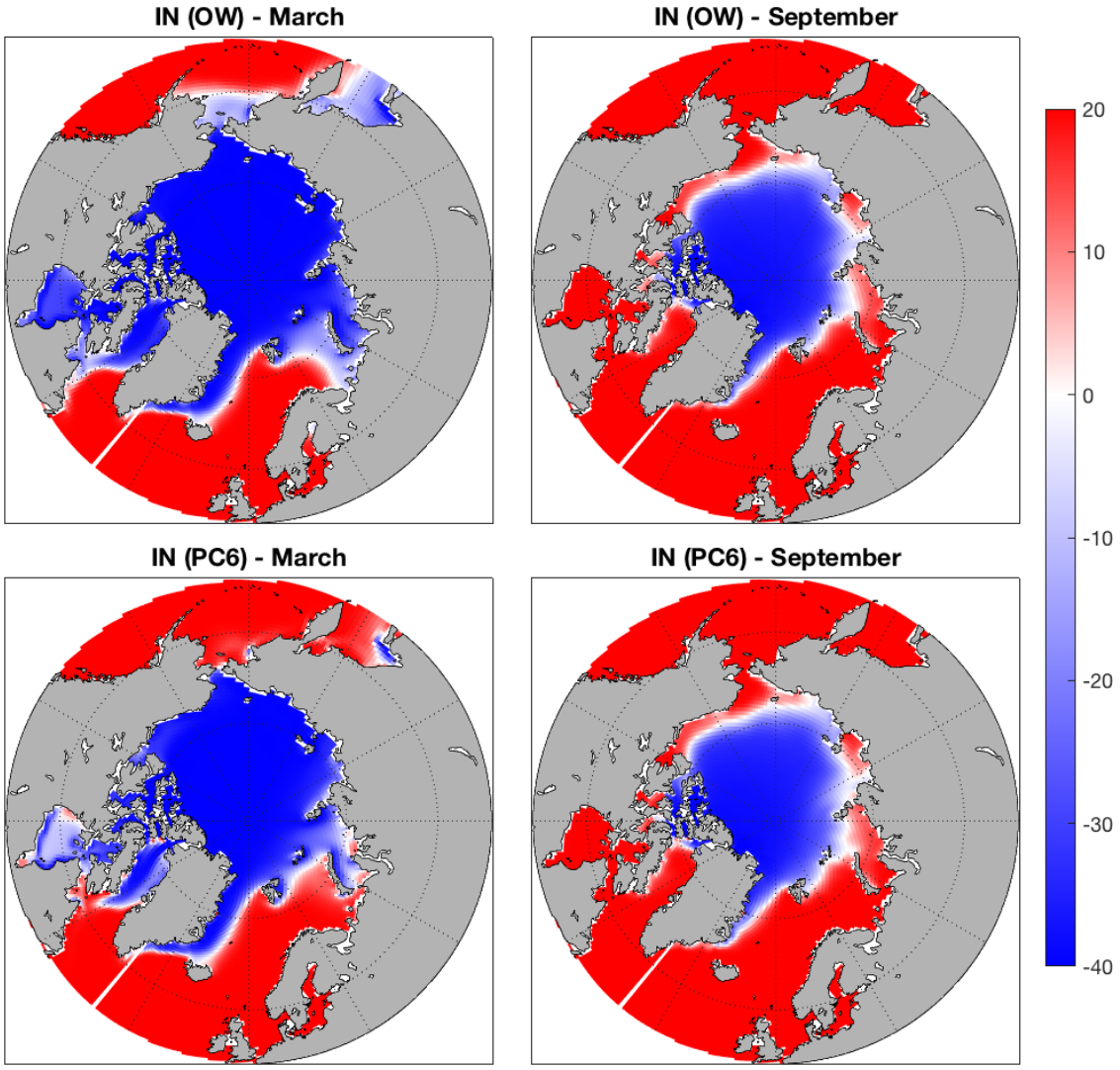

Figure 6: Ice Numeral (IN) LENS ensemble averaged climatology for the period 1960-1999. OW refers to Open Water, a vessel with no ice strengthening. PC6 refers to Polar Class 6, a vessel with moderate ice strengthening. Positive values (red) represent ice conditions where navigation is allowed. Negative values (blue) represent ice conditions where navigation is not permitted.

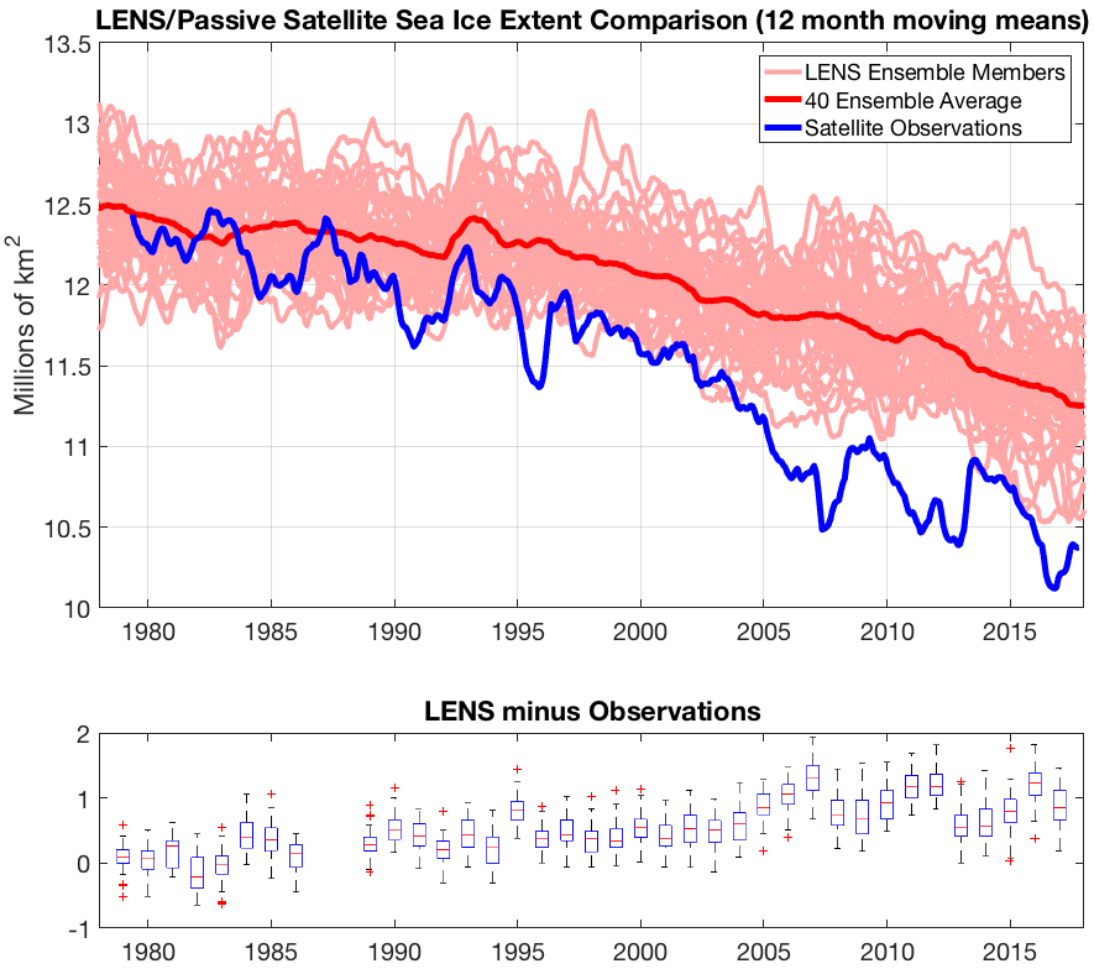

Figure 7:

Top: Comparison of LENS vs. satellite observations (from Sea Ice Index) of SIE.

Bottom: Spread of the difference between LENS and satellite observations of the annual averages among the ensemble members. Gaps are shown when an entire year of data was unavailable.

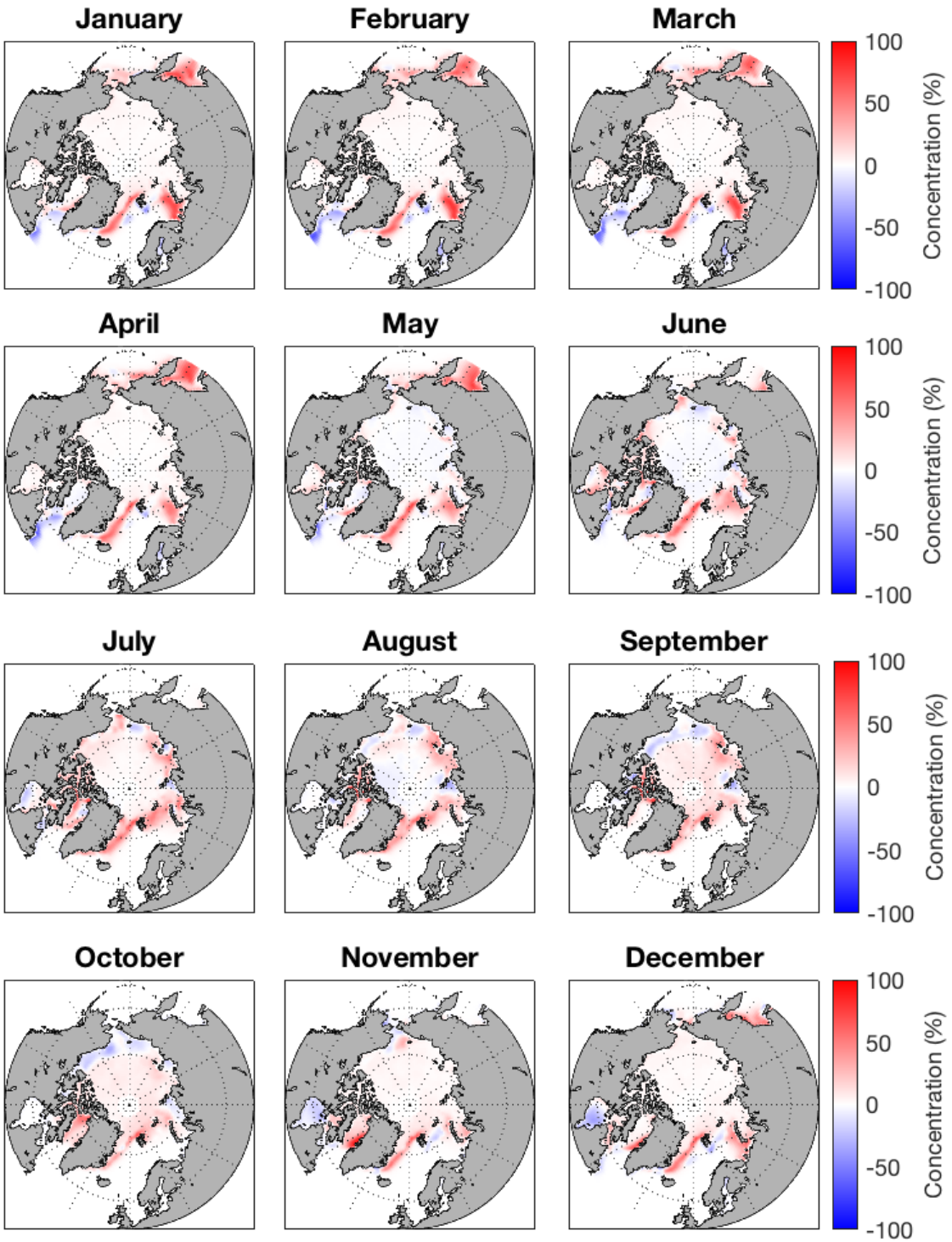

Figure 8: Spatial SIC bias in the LENS ensemble average (LENS minus observations), averaged over the period 1980-99. Red refers to an overestimation, while blue is an underestimation. Note that observations are not available for the area near the pole due to satellite orbit inclination.

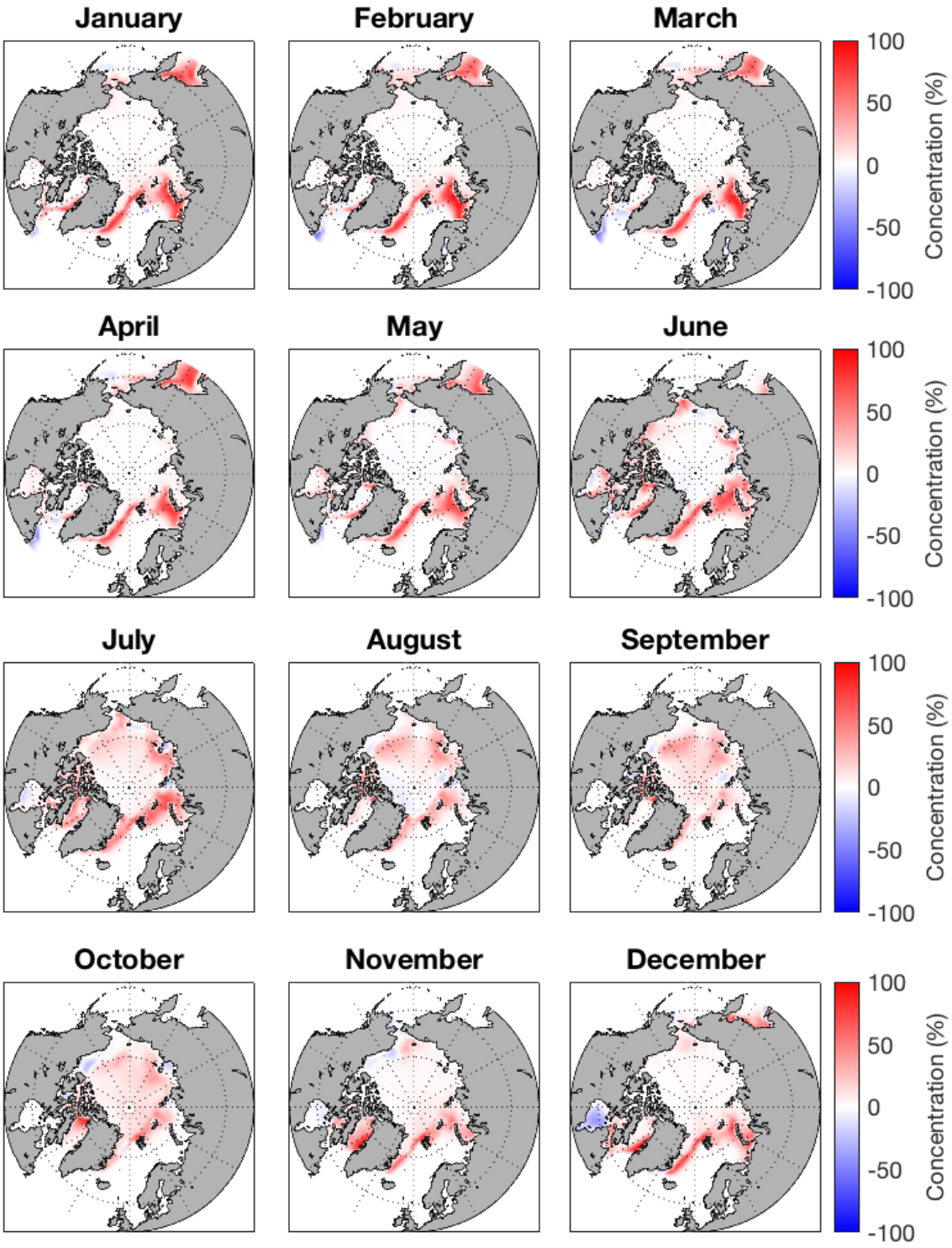

Figure 9: Same as in Figure 8, but for 2000-17.

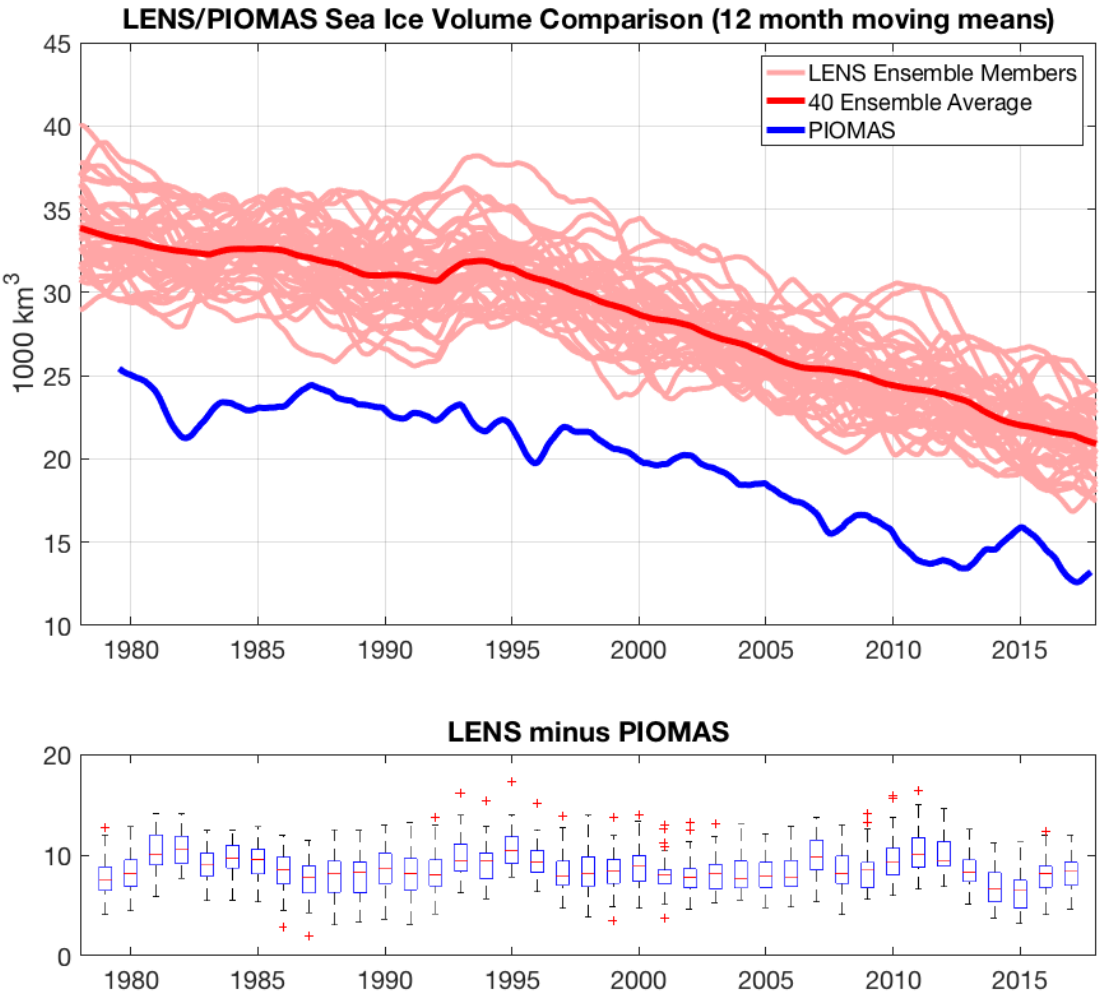

Figure 10: Same as in Figure 2, but for volume comparison with PIOMAS.

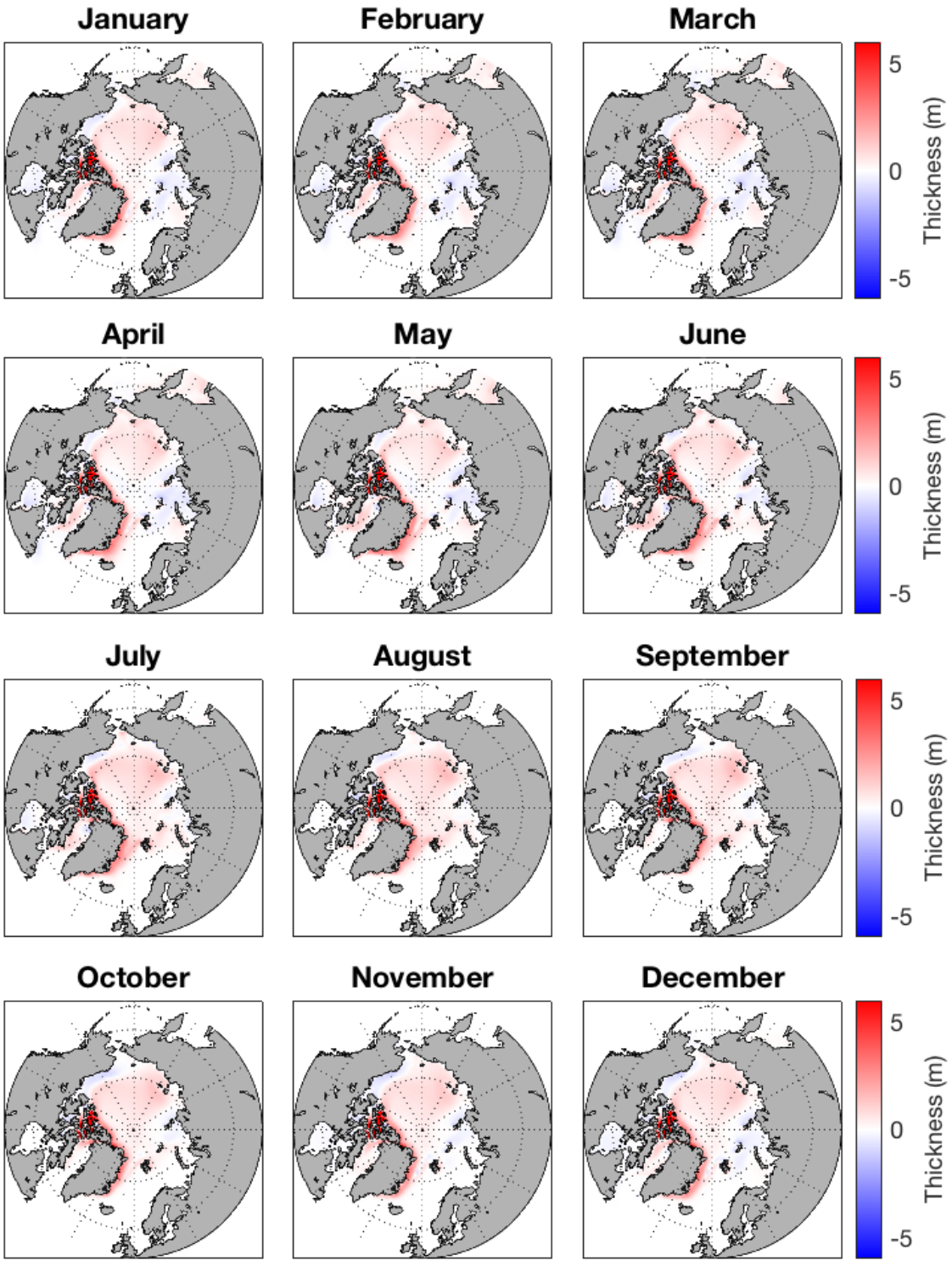

Figure 11: Spatial SIT bias in the LENS ensemble average (LENS minus PIOMAS), averaged over the period 1980-99. Red refers to an overestimation, while blue is an underestimation.

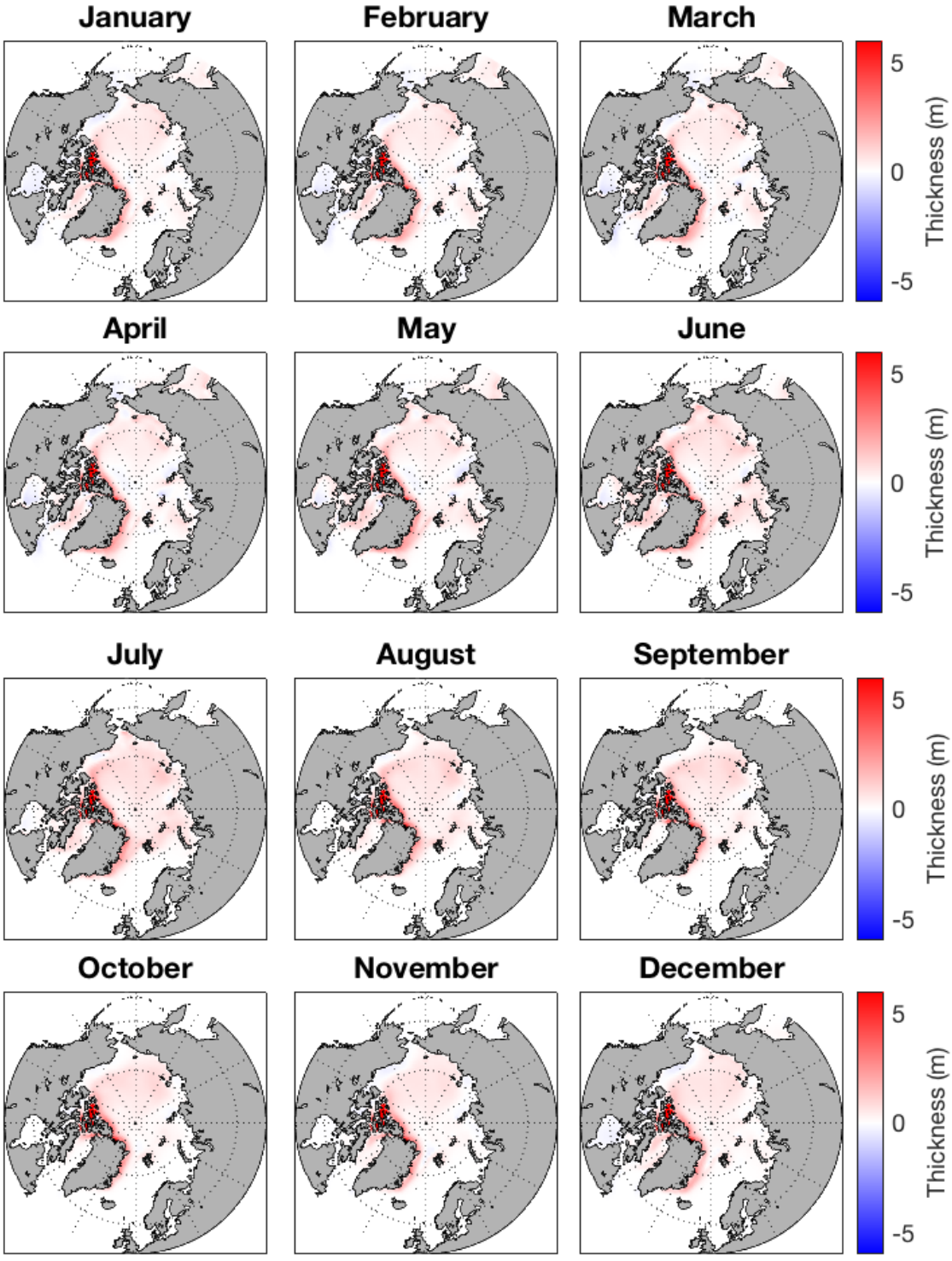

Figure 12: As in Figure 6, but for 2000-17.

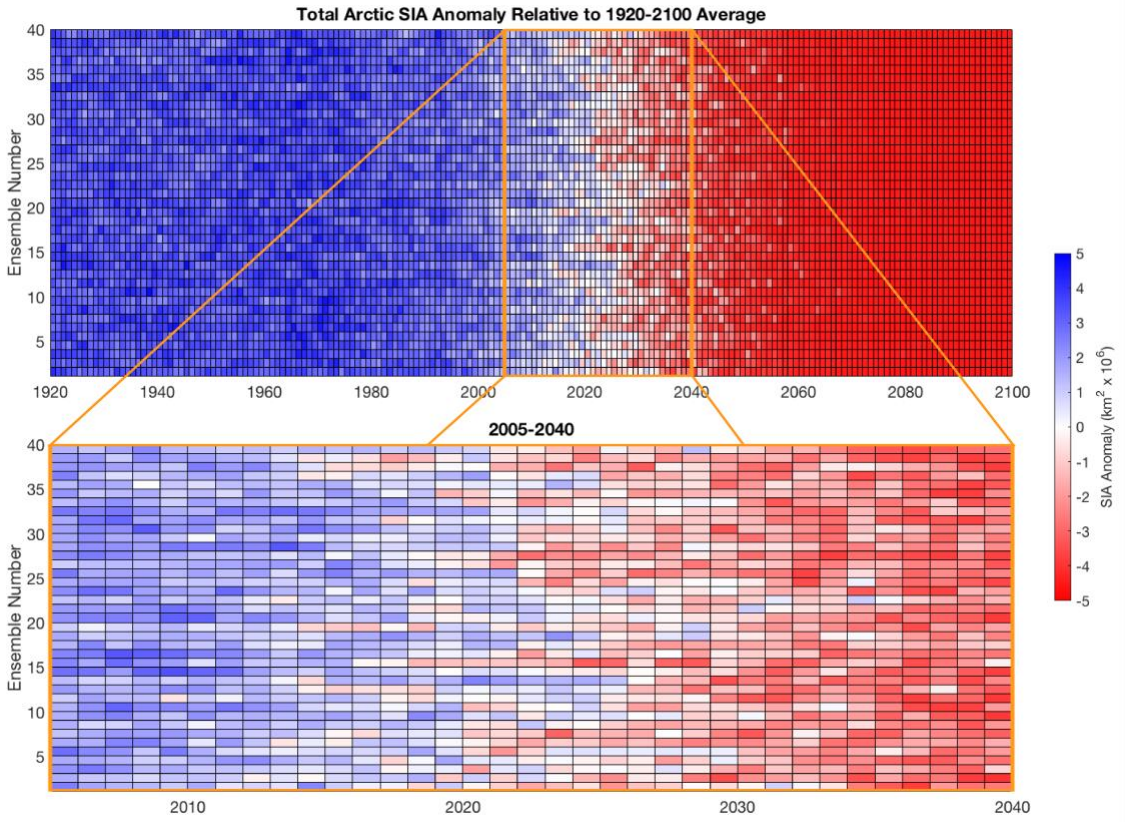

Figure 13: Checkerboard plots of September total SIA for each of the 40 ensemble members. SIA is presented as an anomaly relative to each ensemble's September average from 1920-2100. The bottom plot expands the highly variable period from 2005-2040.

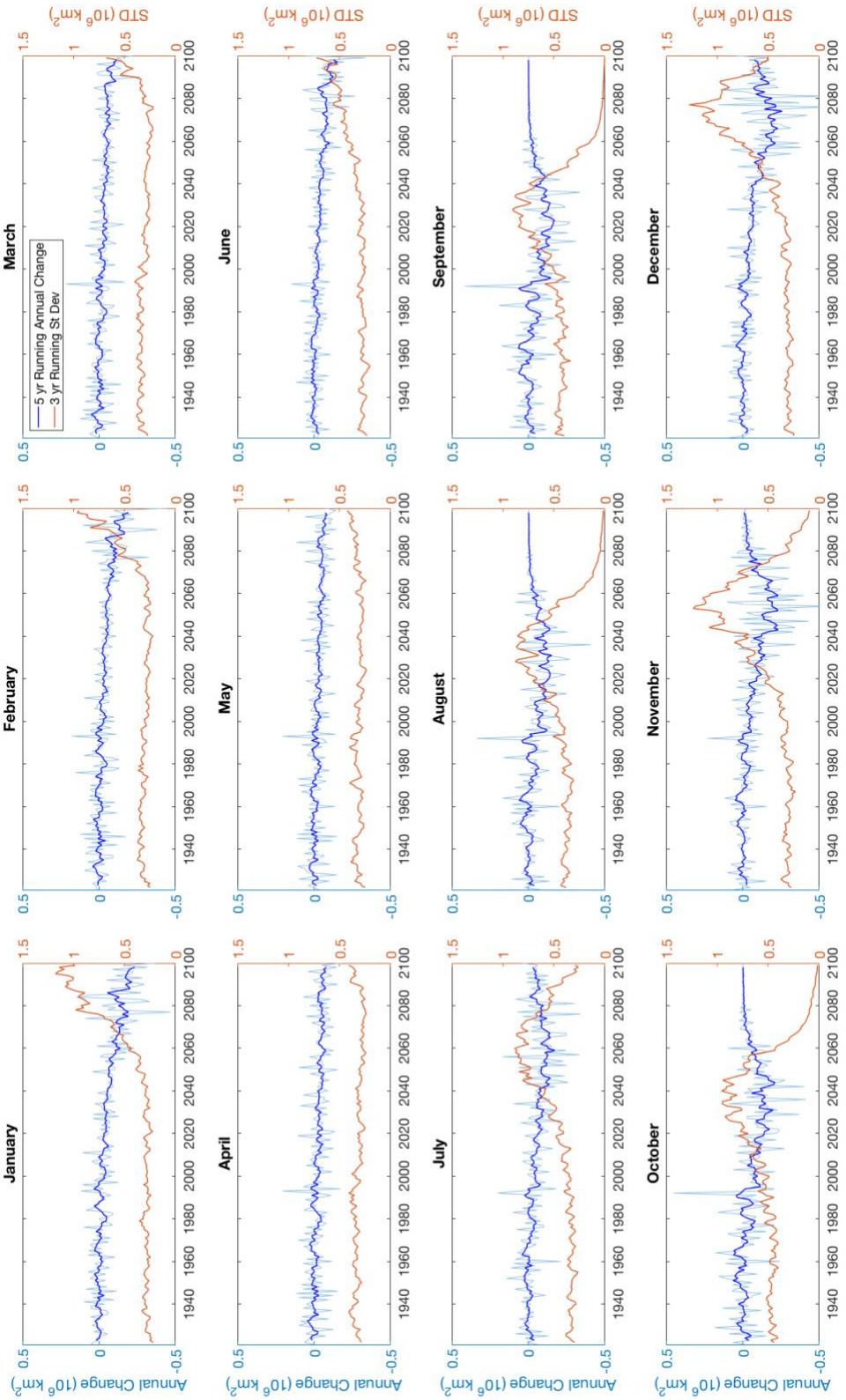

Figure 14: Year-to-year difference (light blue), 5 year running mean (dark blue), and variability expressed as interannual standard deviation (orange) of total SIA.

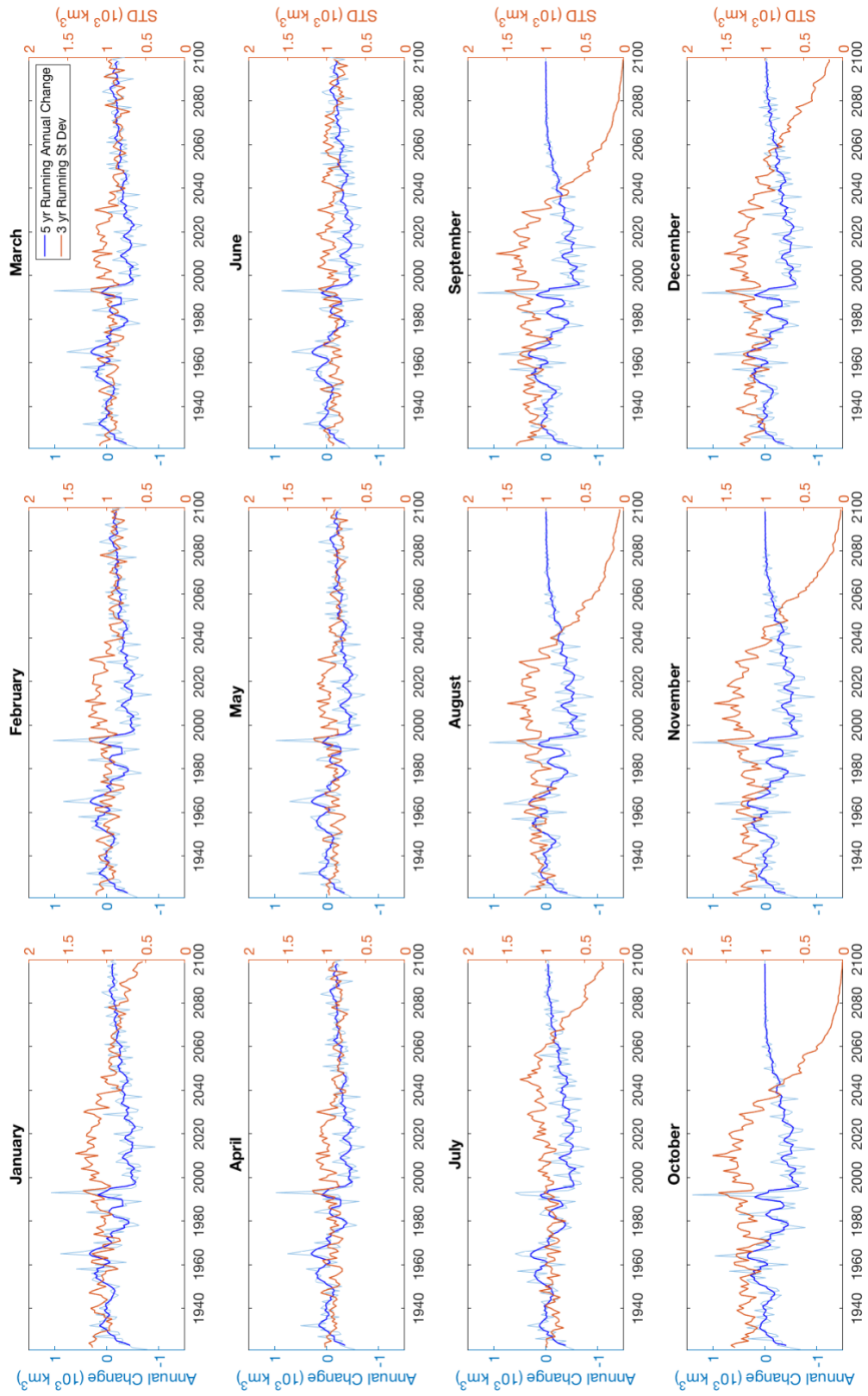

Figure 15: As in Figure 14, but for total SIV.

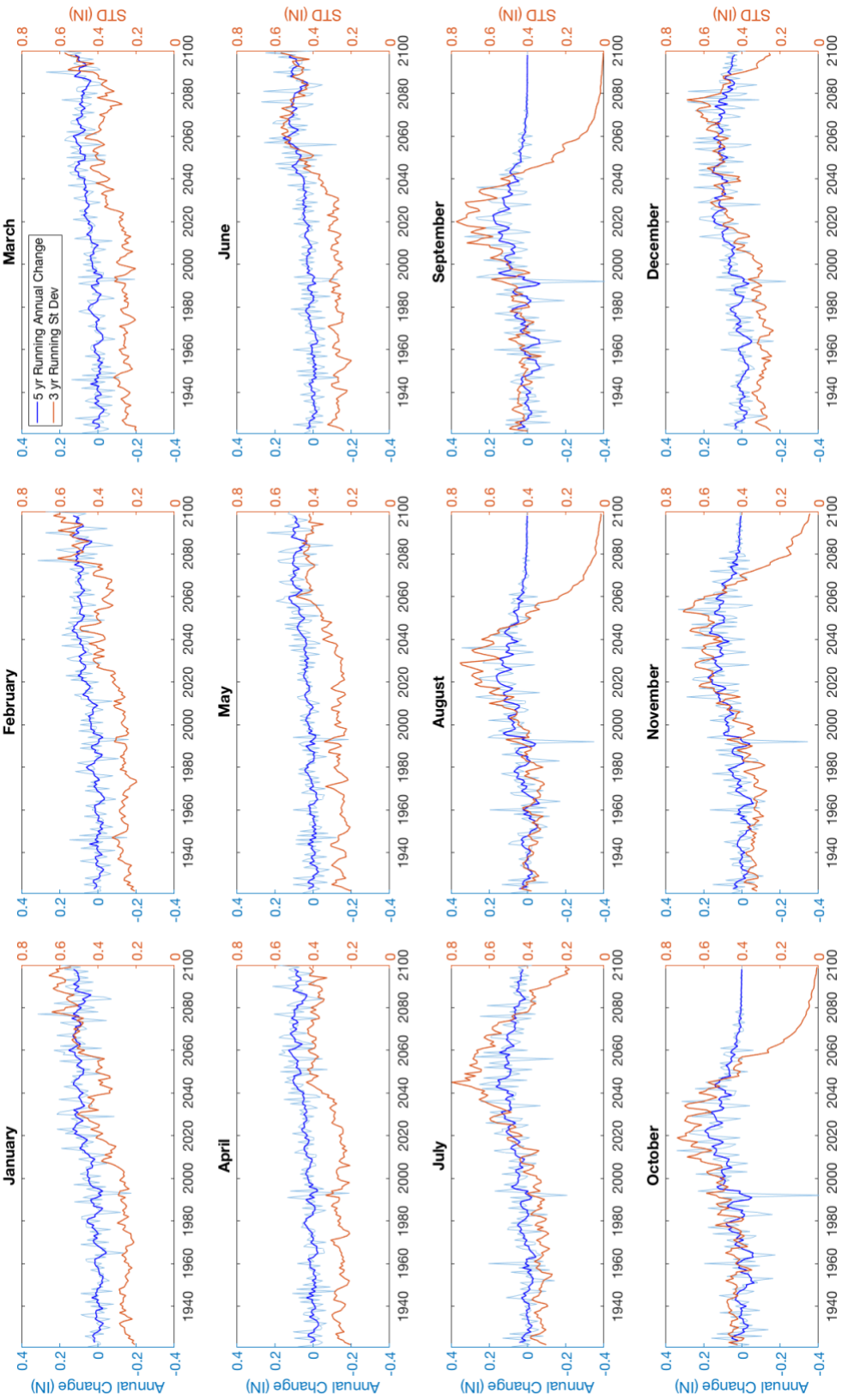

Figure 16: As in Figure 14, but for IN (OW).

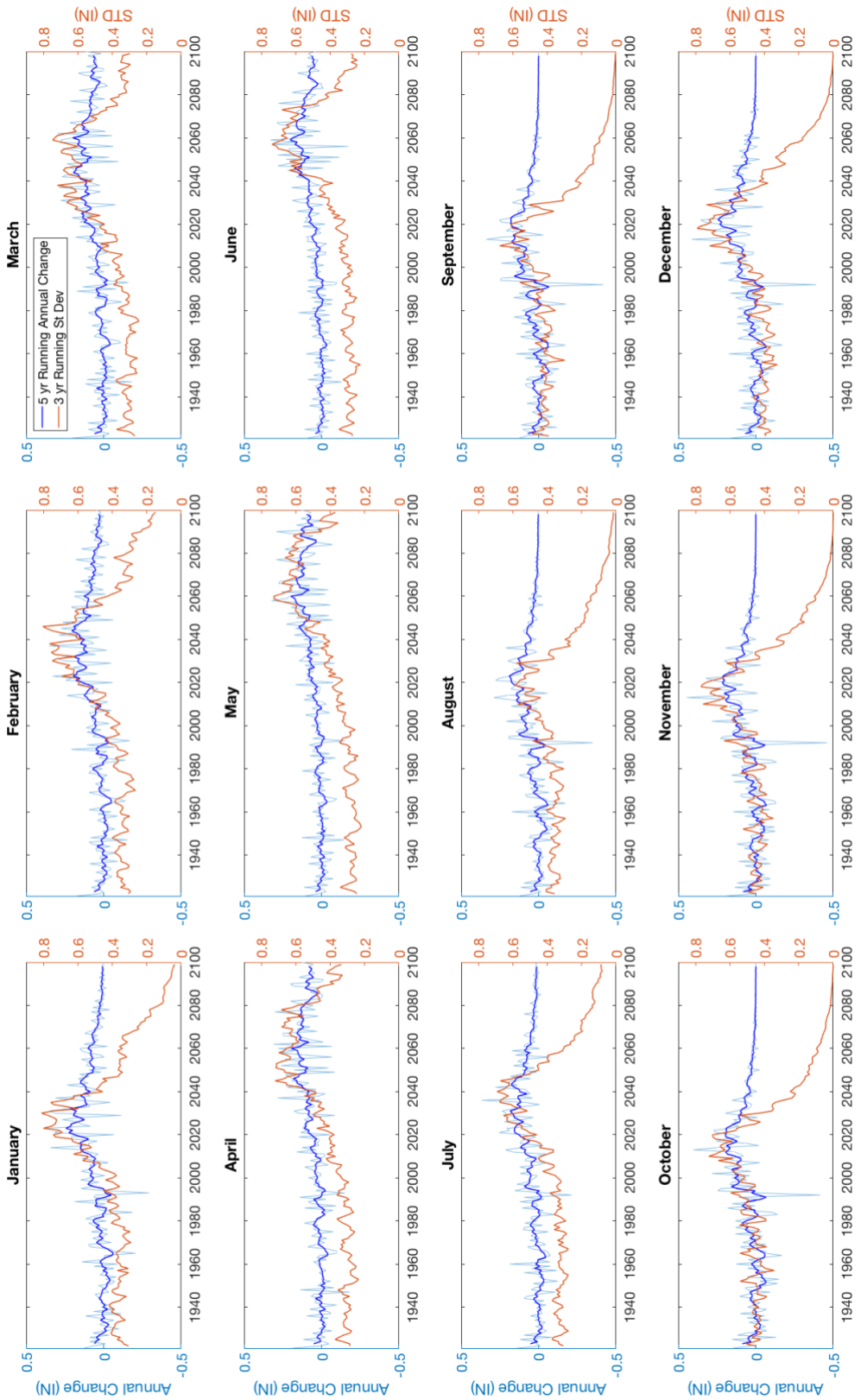

Figure 17: As in Figure 14, but for IN (PC6).

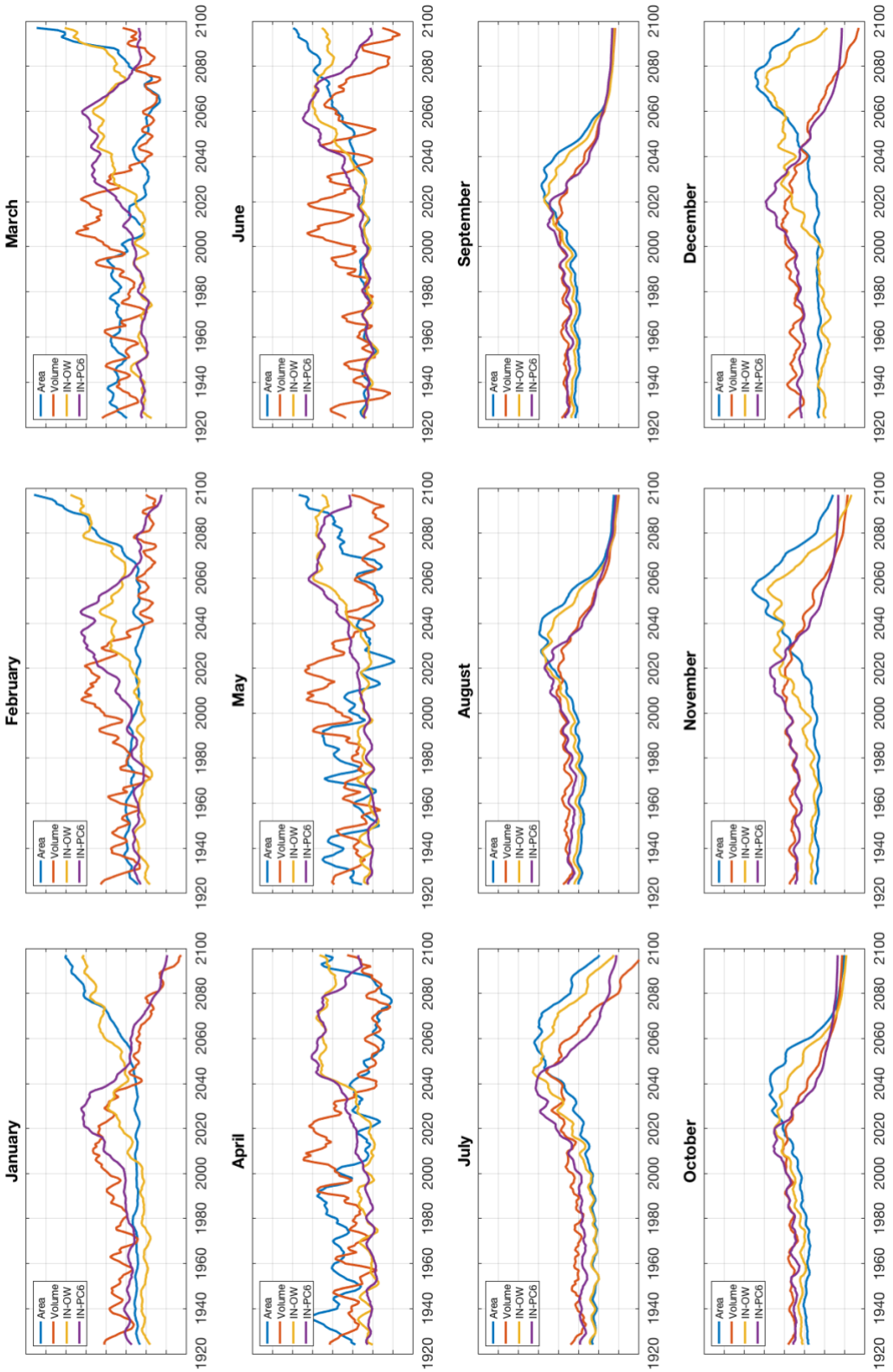

Figure 18: Normalized variability curves of four important sea ice metrics. Variability of different metrics can be compared for amplitude and timeliness in a given month. Amplitudes cannot be compared between months.

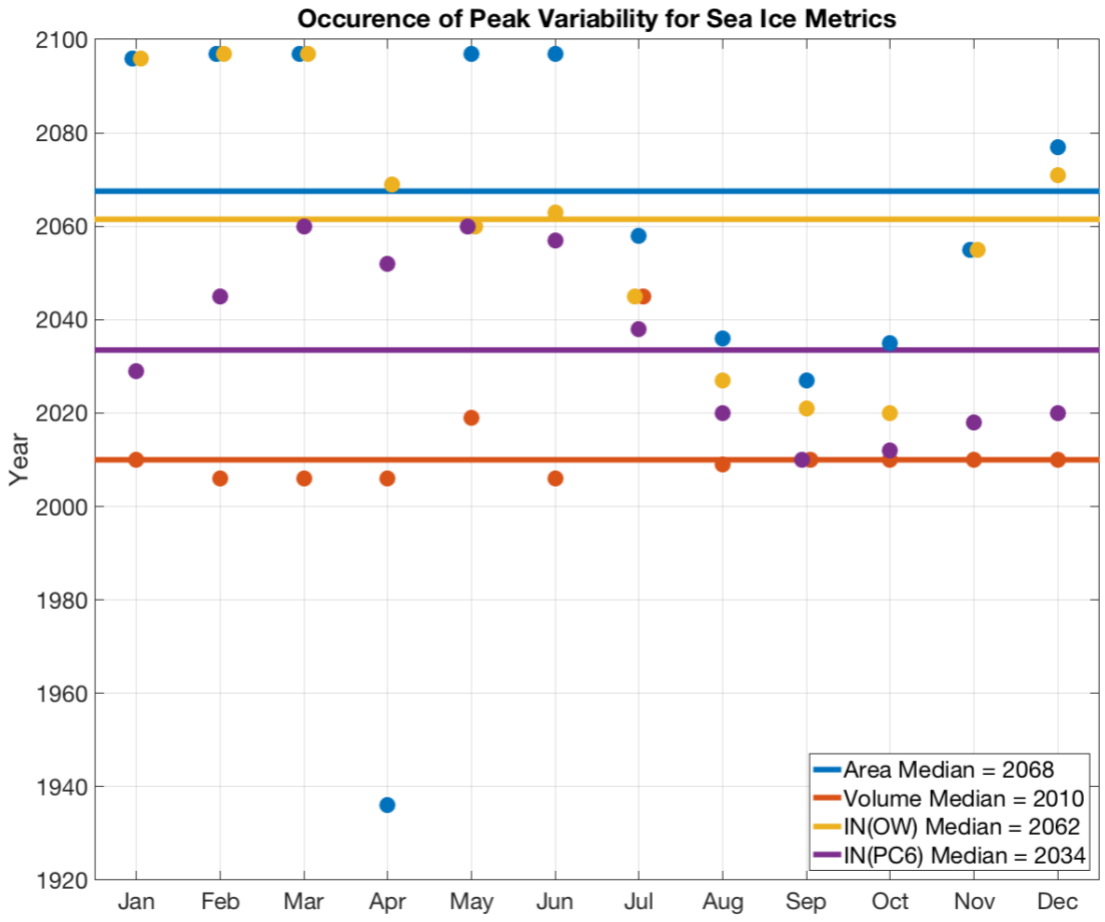

Figure 19: Occurrence of the peak variability of four ice metrics, for each month from the LENS run. Lines represent median occurrences among all ensemble members (values listed in legend). Note that scatter points that occur concurrently have been slightly displaced for visibility.

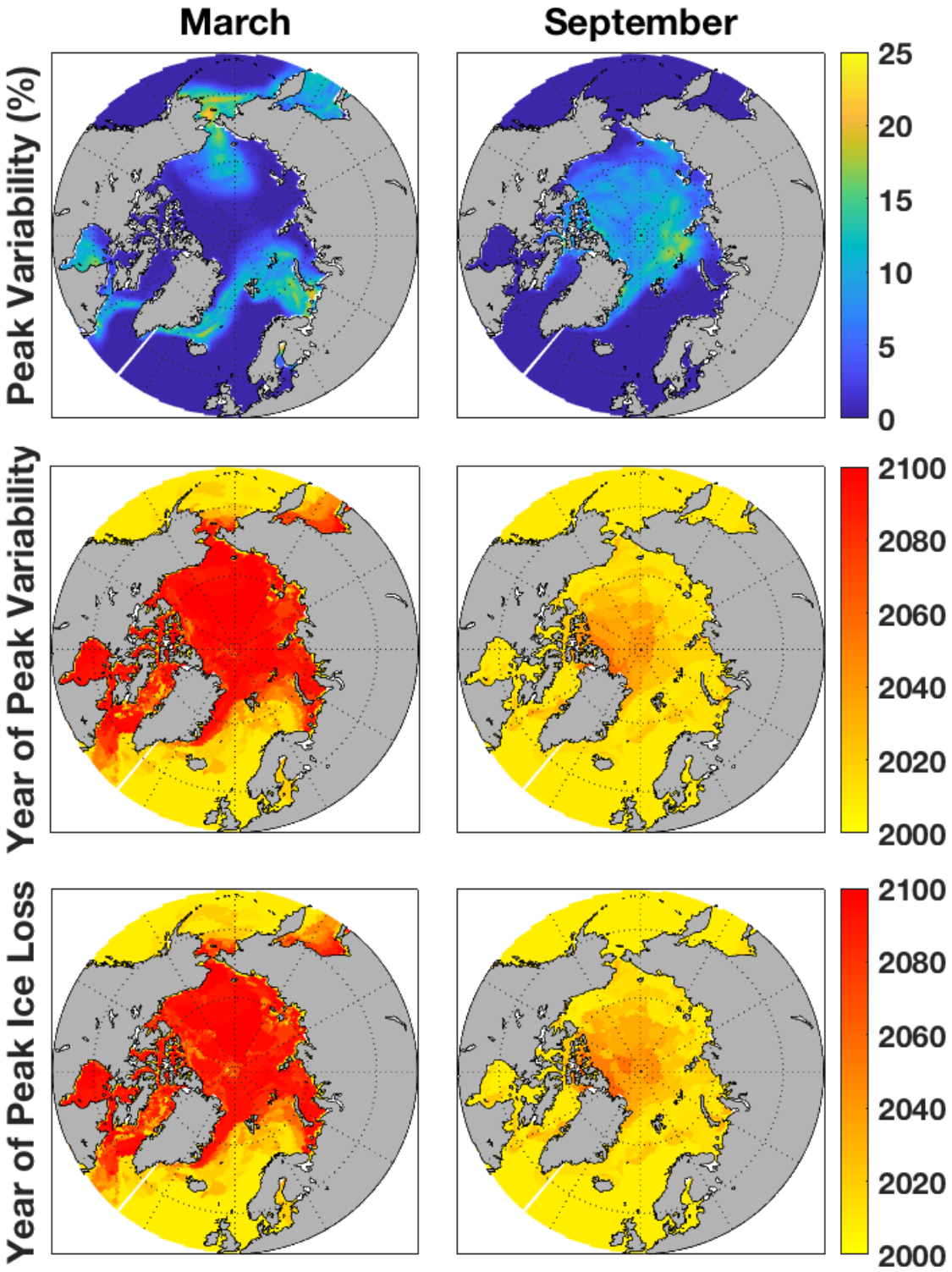

Figure 20: Spatial patterns of peak variability in SIC. The top row represents the magnitude of the peak variability occurring at each grid cell (i.e. the 3-year running mean of the year-to-year difference). The middle row is the year corresponding to the peak occurrence. The bottom row is the year associated with peak rate of concentration loss. Plots display the month of March (left column) and September (right column).

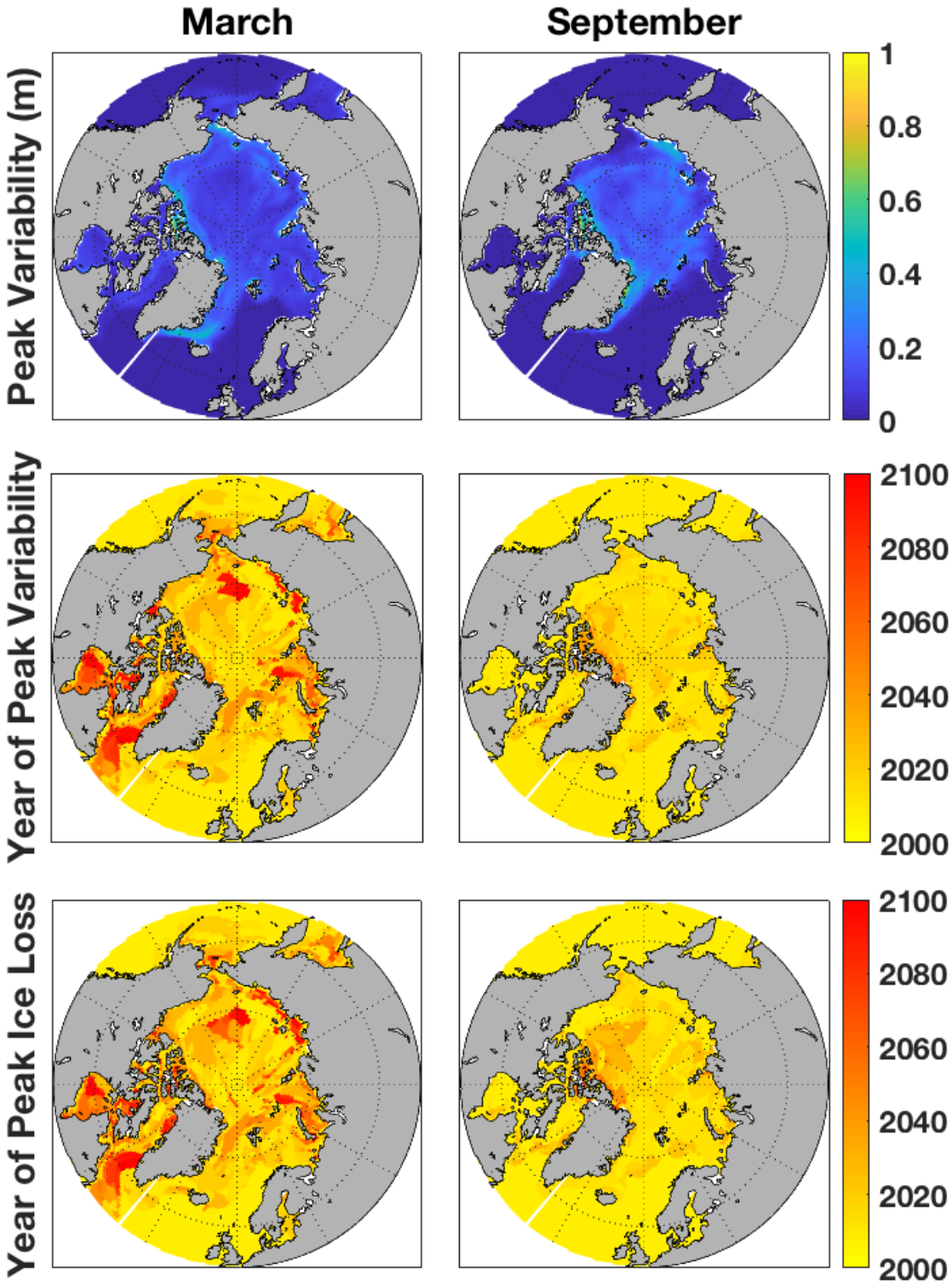

Figure 21: Same as in Figure 20, but for SIT.

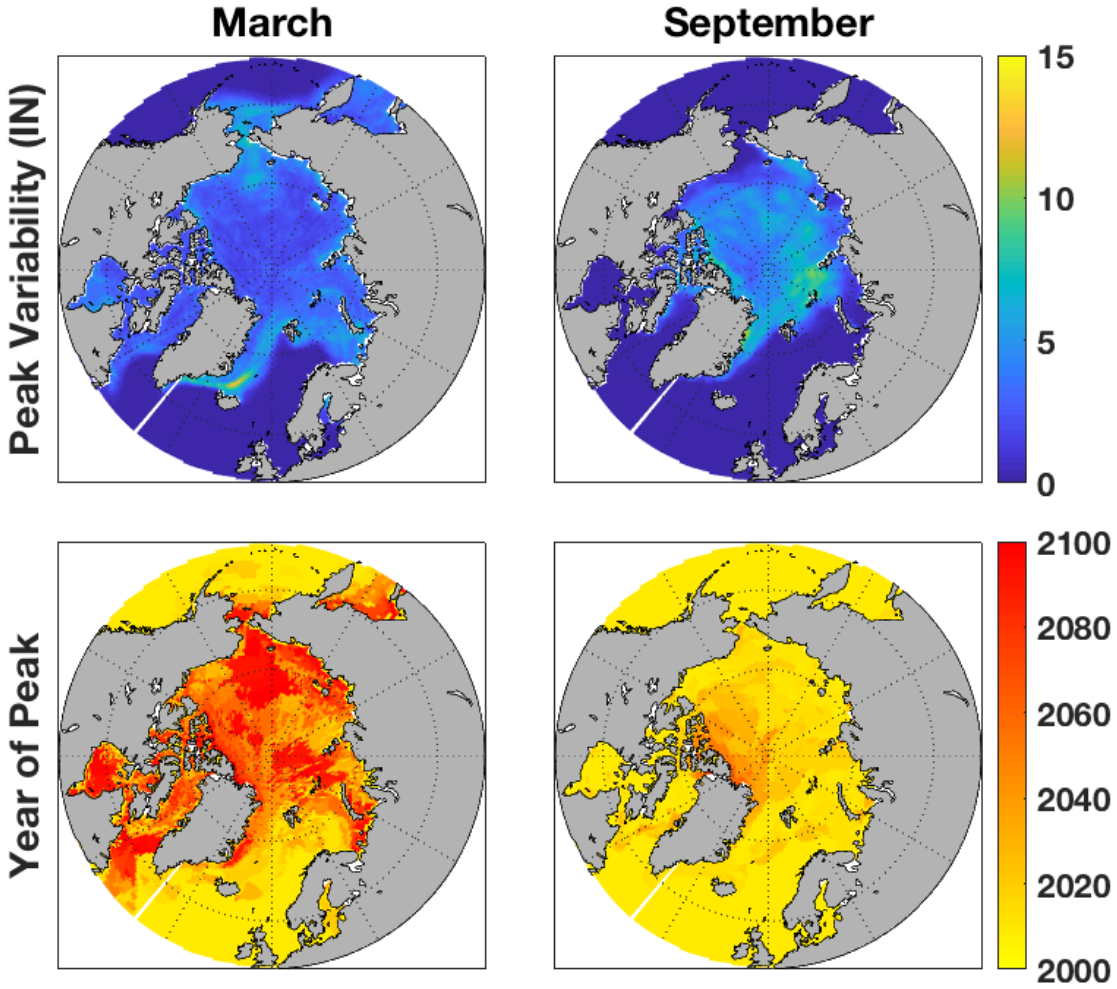

Figure 22: Same as in Figure 20, but for IN (OW).

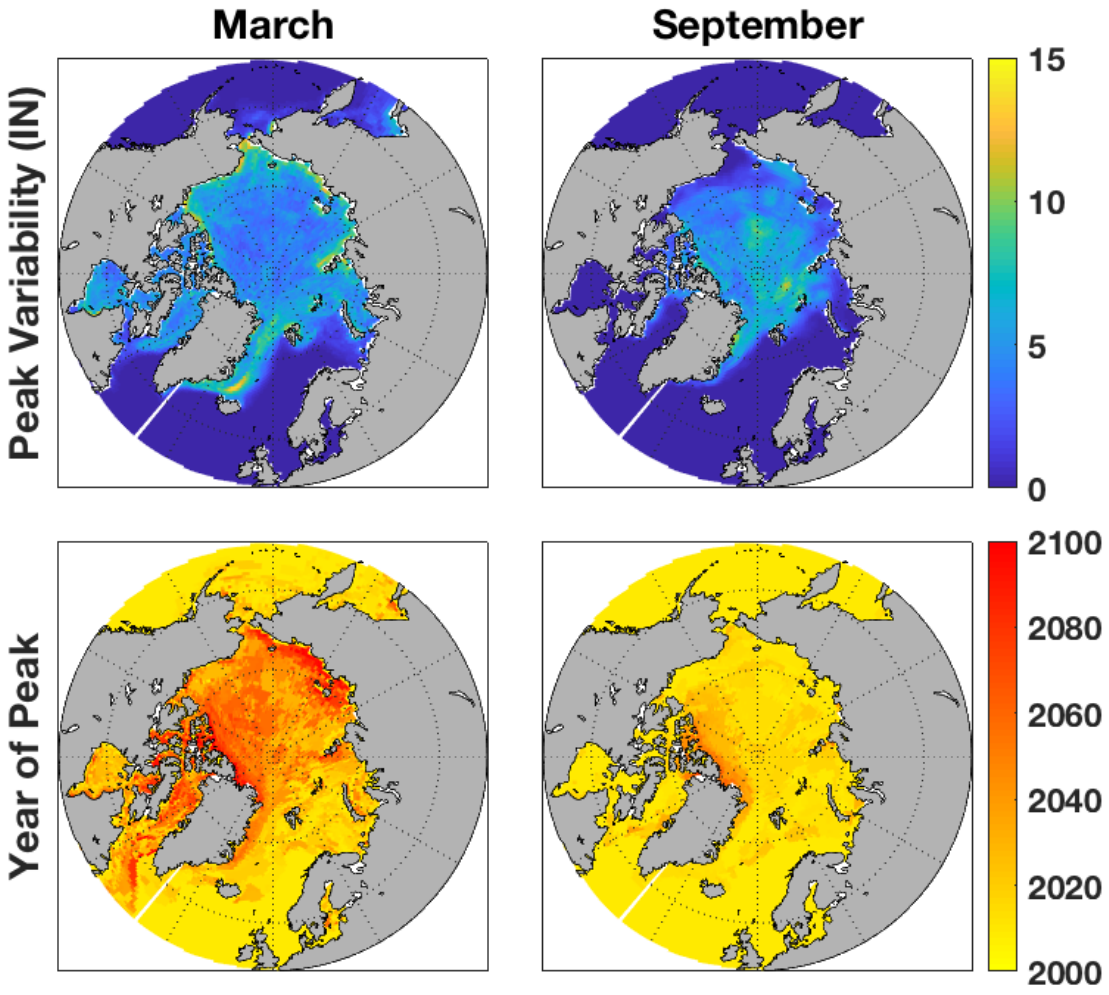

Figure 23: Same as in Figure 20, but for IN (PC6).

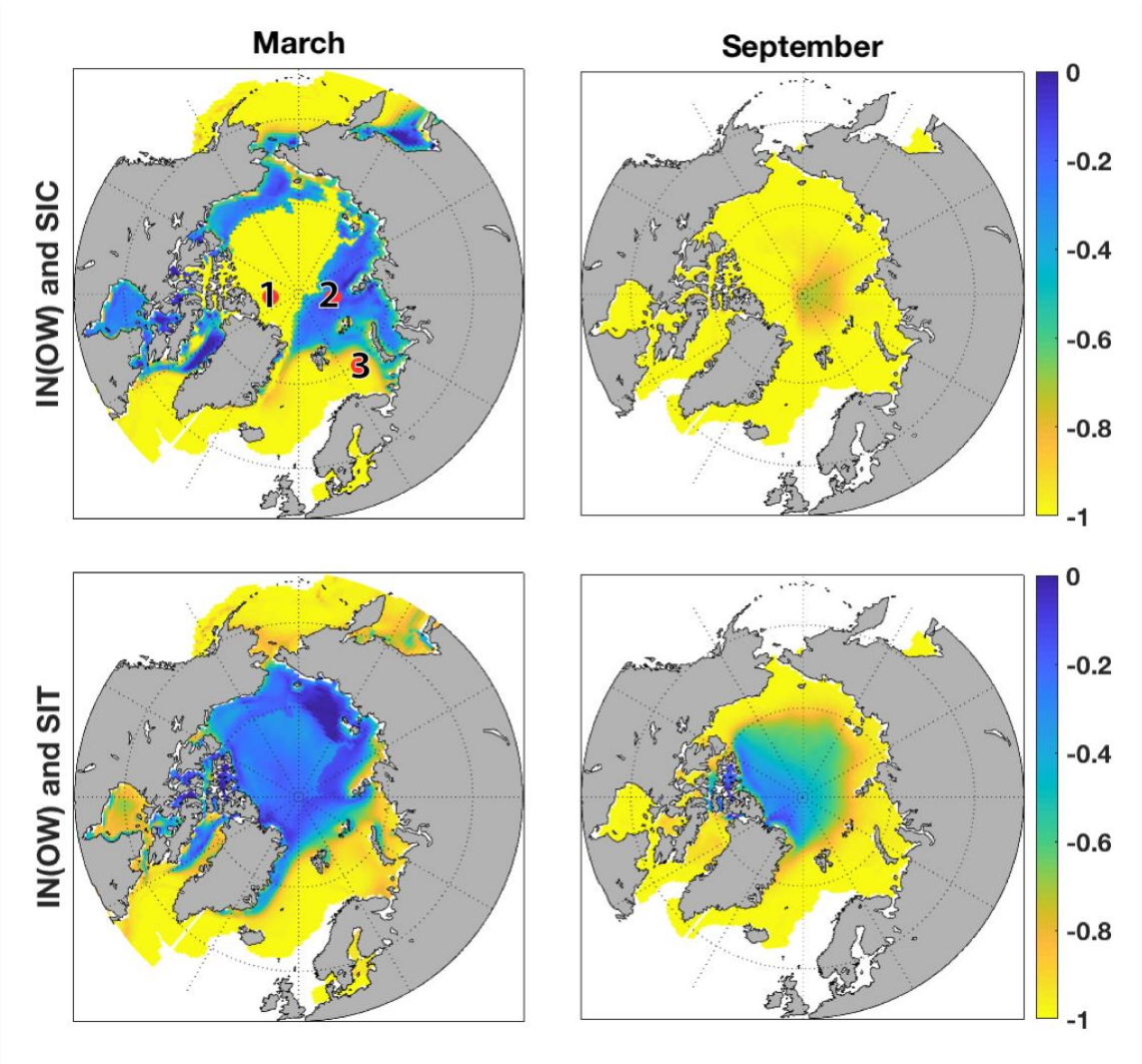

Figure 24: Each map plots correlation coefficients of IN (OW) with either SIC (top plots) or SIT (bottom plots), for the time period 1920-2005 (historical portion of LENS run). The plots on the left are for March and the plots on the right are for September. Plots are not averaged in any way, i.e. each temporal and ensemble point for the respective spatial points are included in the regression. The red circles represent the points referenced by Table 5 and Figures 25-28.

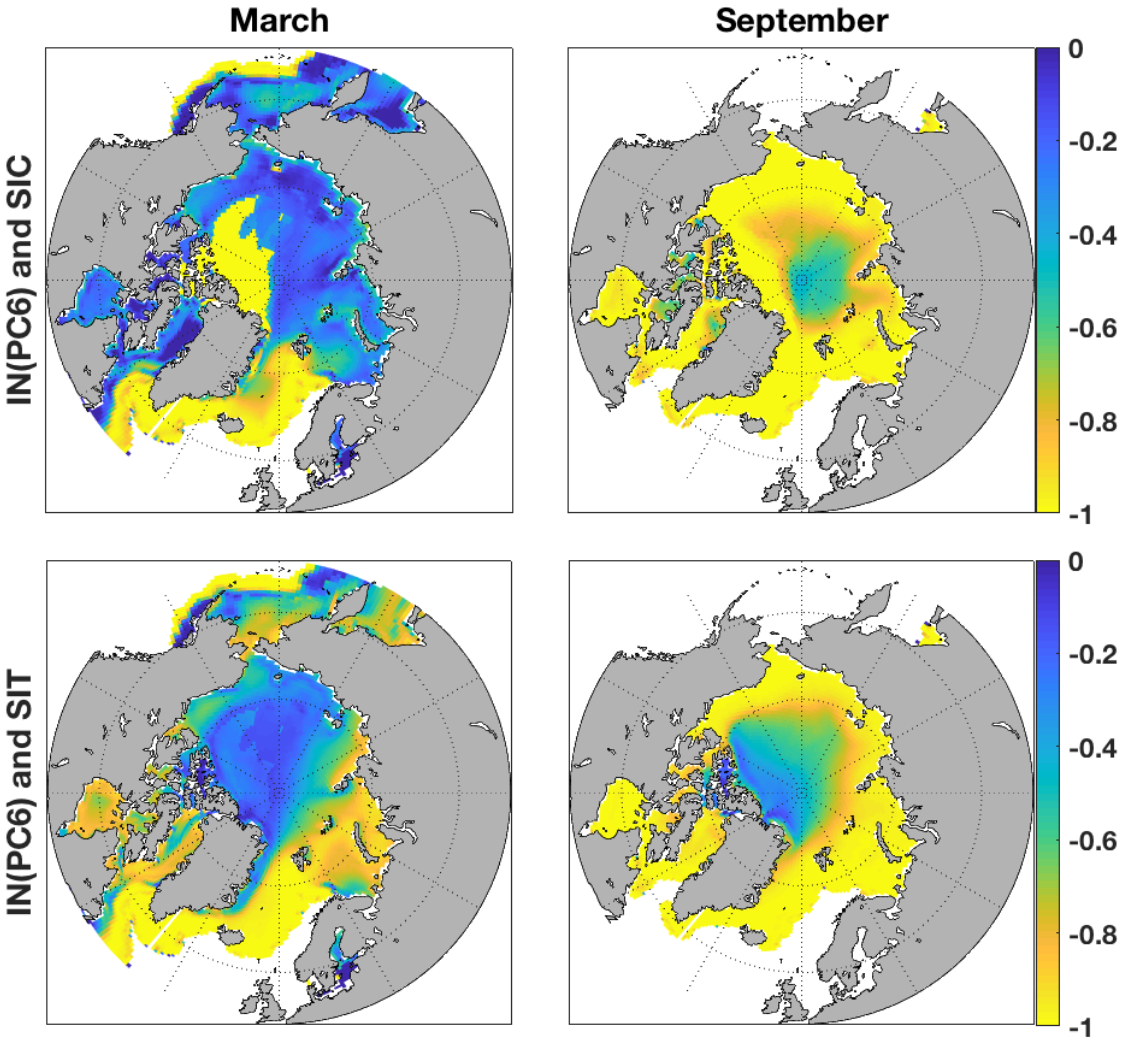

Figure 25: Same as in 24, but for Polar Class 6 (PC6).

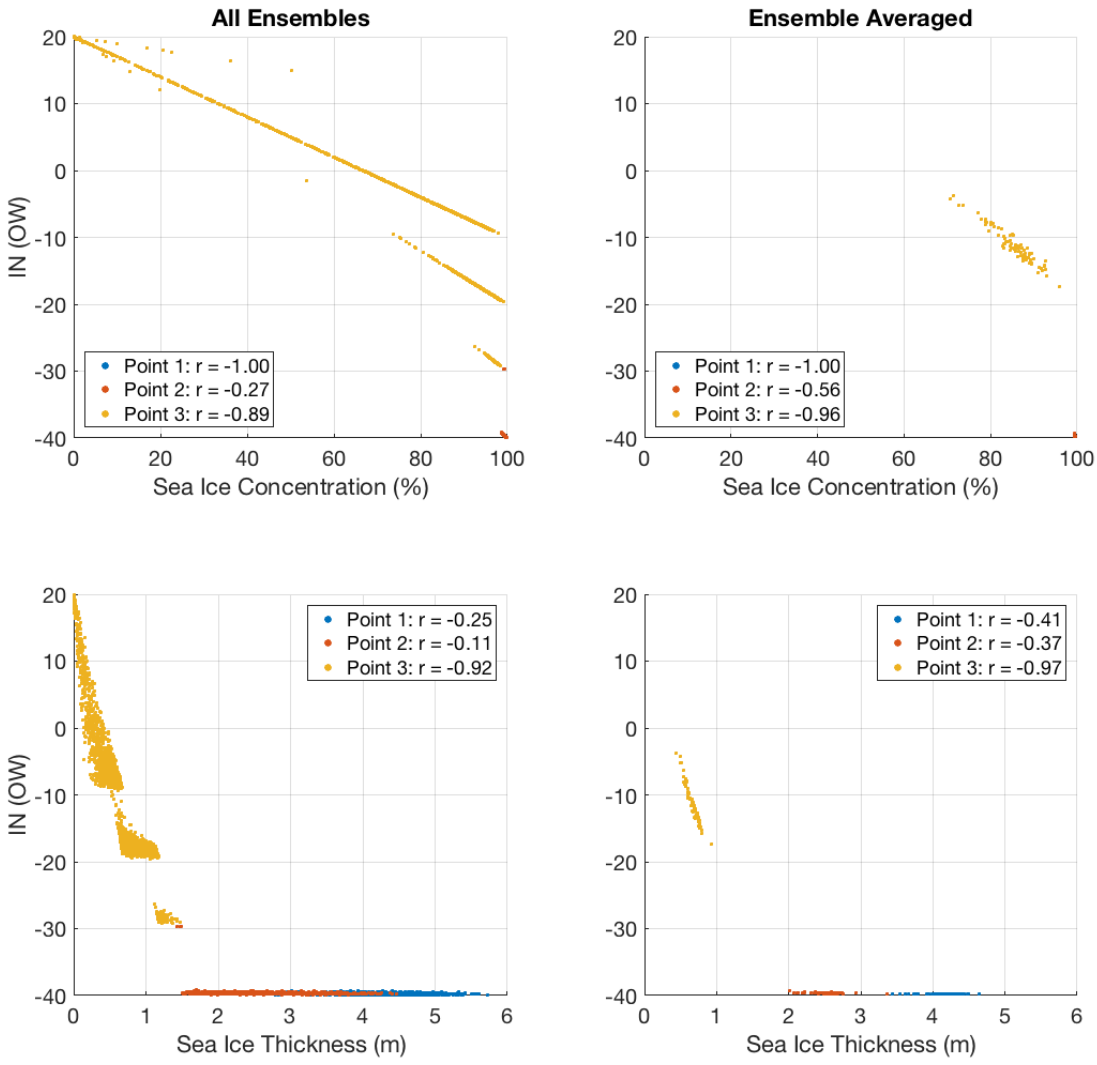

Figure 26: Scatter plots of IN (OW) and components (SIC on top rows, SIT on bottom row), for the month of March. The left column plots show all years and ensembles, the right column shows ensemble averaged points. See Table 5 and Figure 24 for geographic positions of the three points featured on plots. The scatter points correspond to the left column of Figure 24. Note that for SIC (top row) all scatter points from geographic point 1 (blue) are clustered at 100% concentration and -40 IN, as are most of point 2 (red).

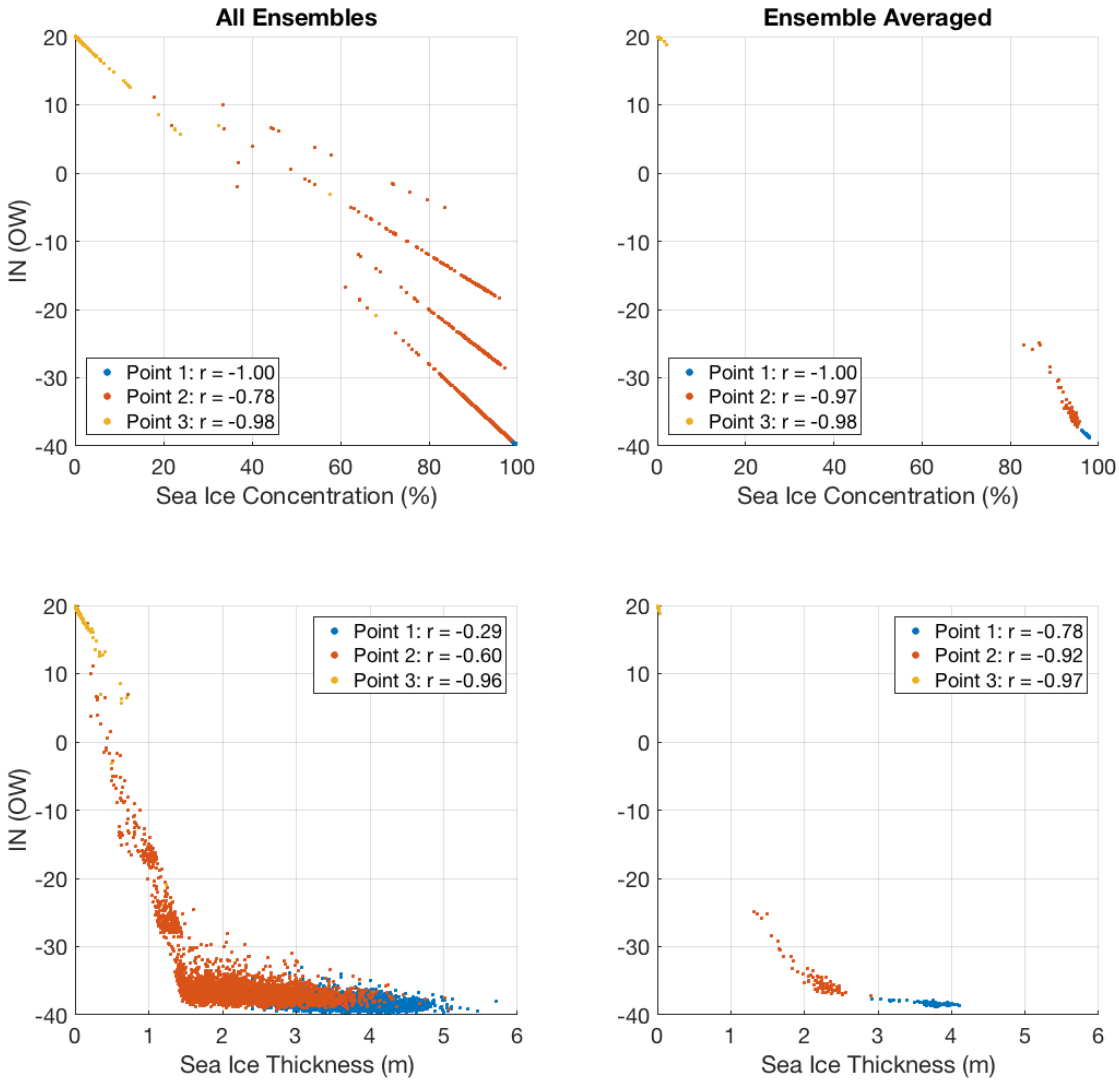

Figure 27: Same as in Figure 26, but for the month of September. The scatter points correspond to the right column of Figure 24.

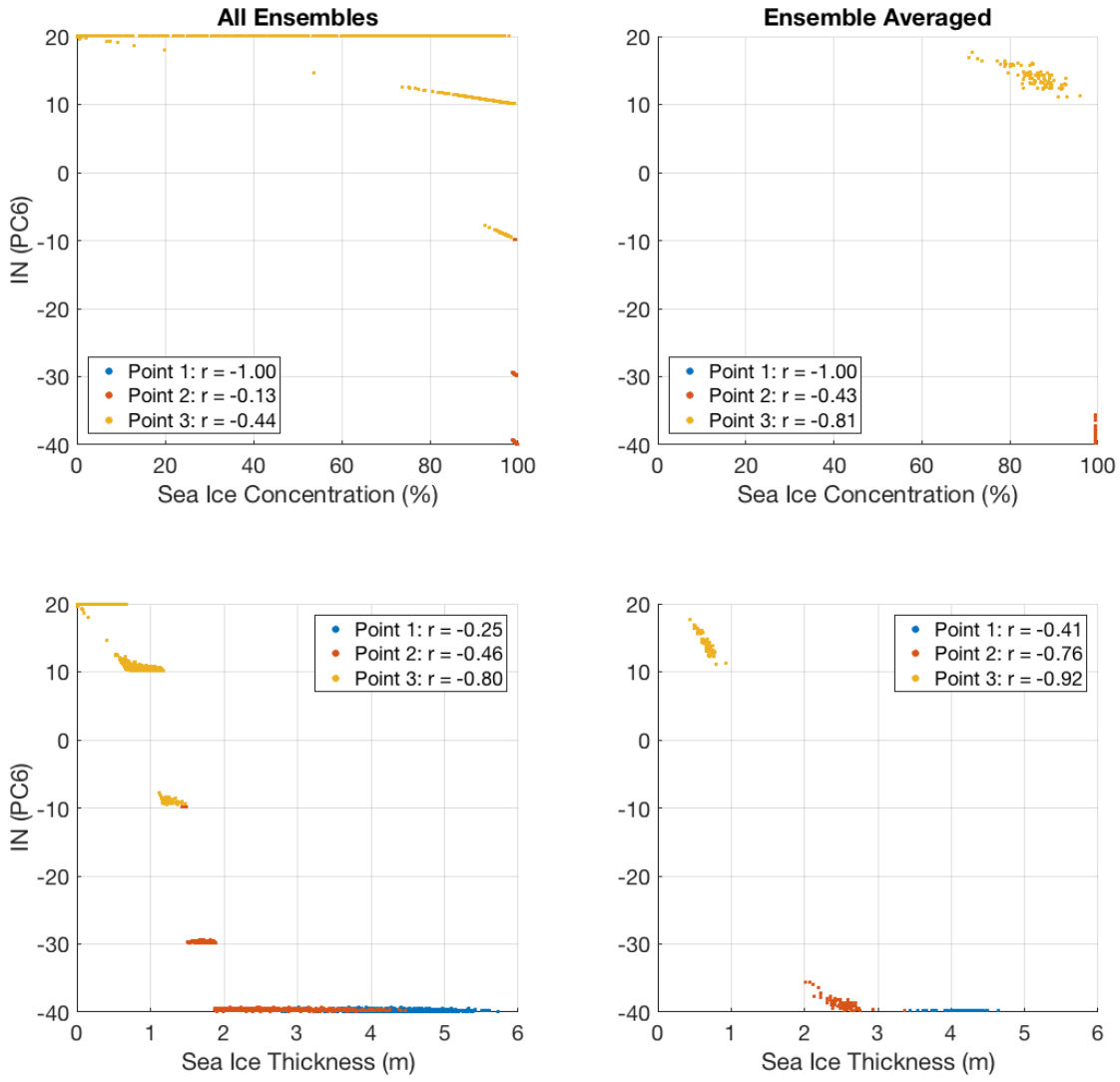

Figure 28: Same as in Figure 26, but for a Polar Class 6 (PC6) vessel, for the month of March. The scatter points correspond to the left column of Figure 25.

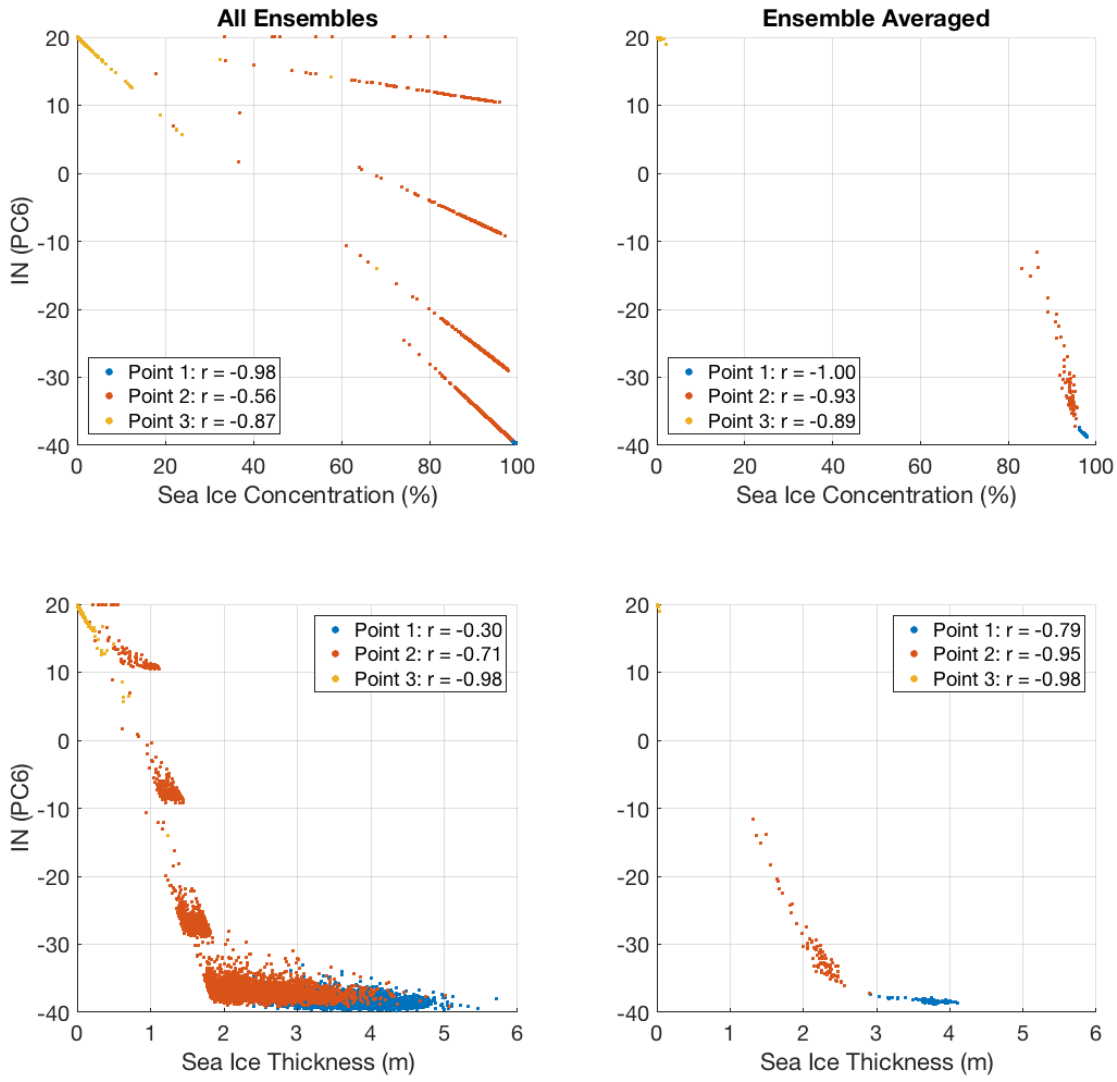

Figure 29: Same as in Figure 26, but for a Polar Class 6 (PC6) vessel, for the month of September. The scatter points correspond to the right column of Figure 25.

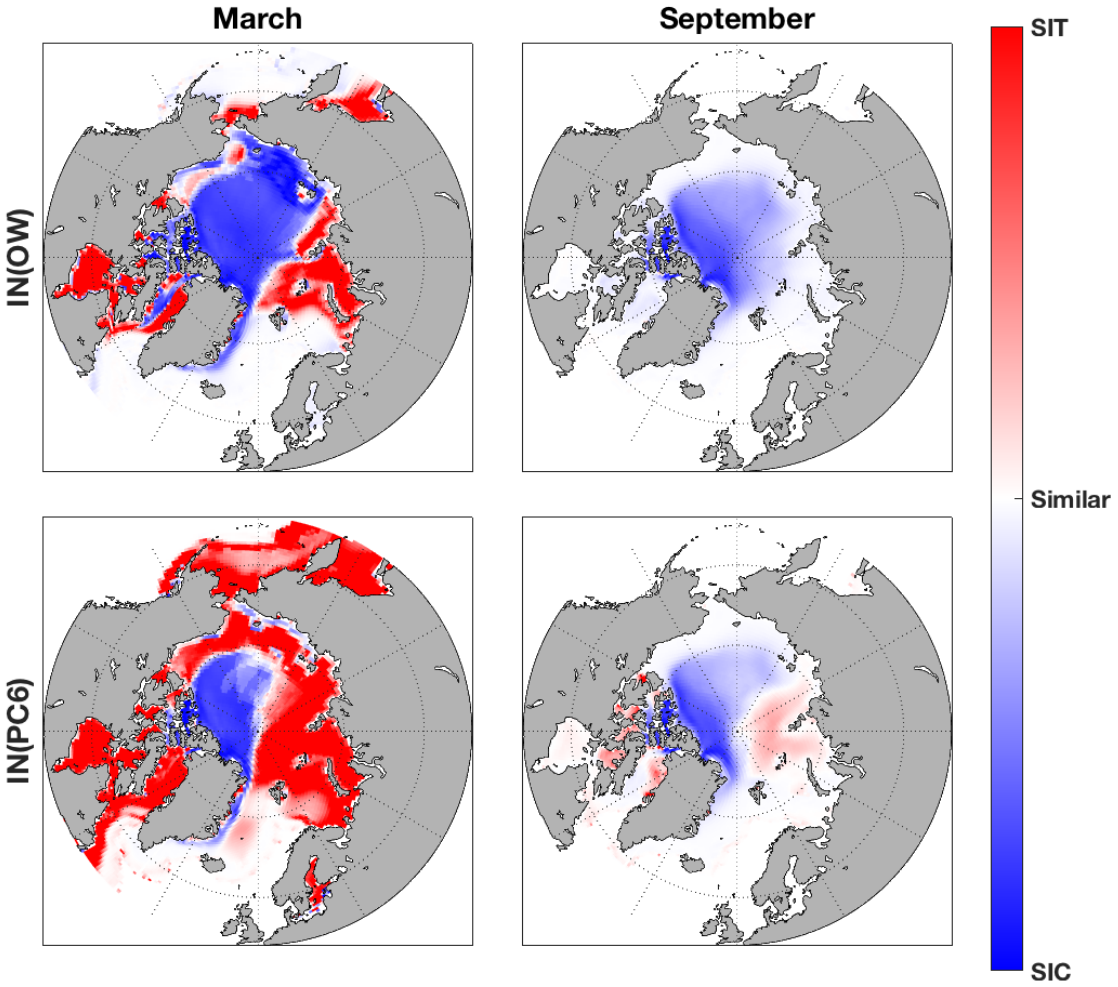

Figure 30: Relative strength of correlations between IN and its components (SIC/SIT). Plots display the ratio of SIT correlation with IN to the correlation of SIC correlation with IN. The color indicates the relative strength of the correlation with each component and white represents ratios of correlation coefficients that are near unity. The top row is for an Open Water vessel (OW) and the bottom row is for a Polar Class 6 vessel (PC6). The left and right columns are for the months of March and September, respectively.

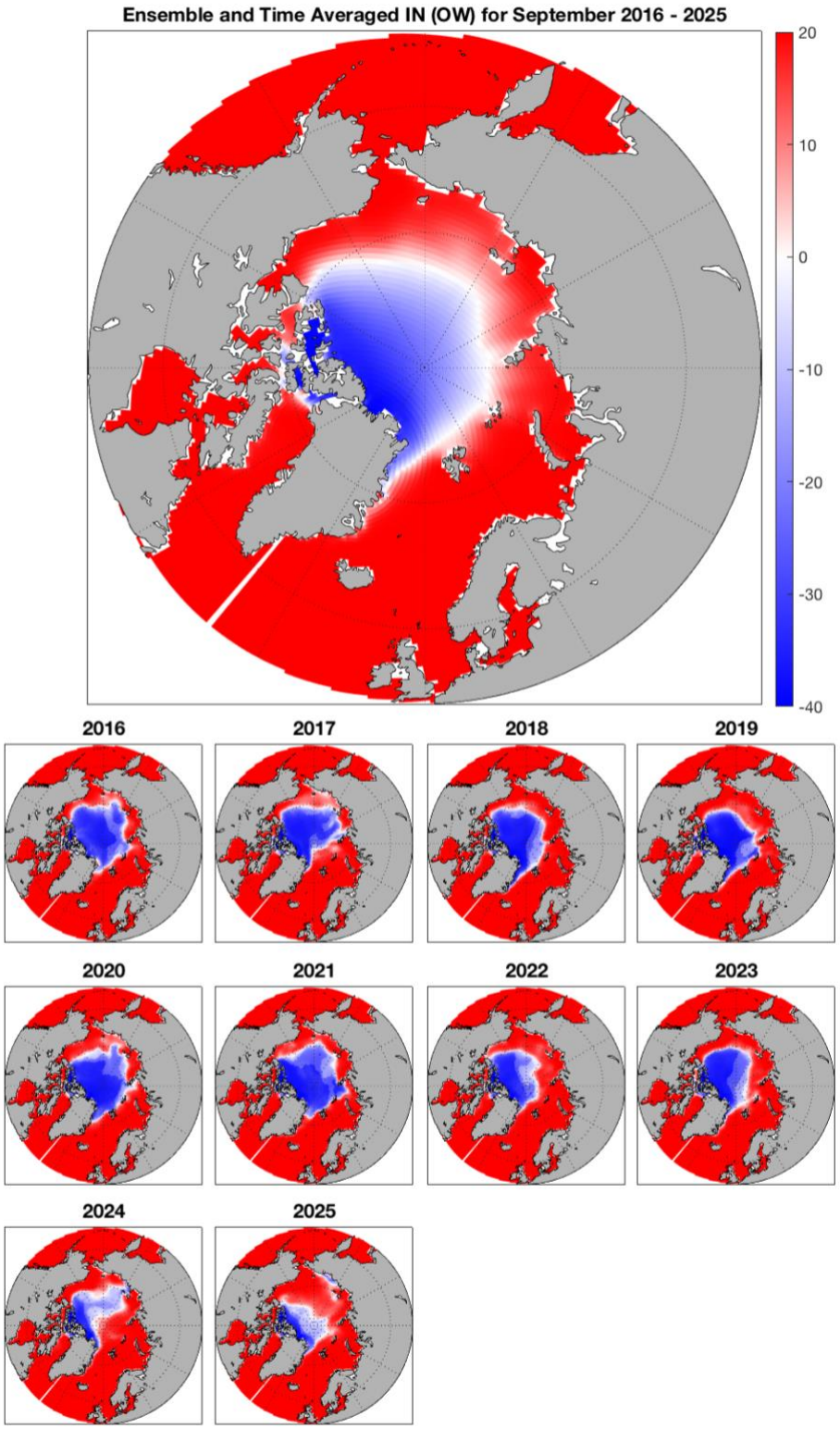

Figure 31: The large plot displays the ensemble and decadal average of IN for an Open Water (OW) vessel, from 2016 to 2025 in September. Note that the Eurasian coast is, on average, favorable for navigation through the Northern Sea Route (NSR) during this period. The smaller plots show each September for only ensemble member 17, during the same period. Note that the NSR opens and closes multiple times during this period.

References

Aksenov, Y., Popova, E. E., Yool, A., Nurser, A. J. G., Williams, T. D., Bertino, L., & Bergh, J. (2017). On the future navigability of Arctic sea routes: High-resolution projections of the Arctic Ocean and sea ice. *Marine Policy*, *75*, 300–317. https://doi.org/10.1016/j.marpol.2015.12.027

Bitz, C. M., & Stroeve, J. (2014). Arctic sea ice predictability. *Variations*, *12*(3), 24–27.

Cao, Y., Liang, S., Chen, X., & He, T. (2015). Assessment of Sea Ice Albedo Radiative Forcing and Feedback over the Northern Hemisphere from 1982 to 2009 Using Satellite and Reanalysis Data. *Journal of Climate*, *28*(3), 1248–1259. https://doi.org/10.1175/JCLI-D-14-00389.1

Comiso, J. C., Parkinson, C. L., Markus, T., Cavalieri, D. J., & Gersten, R. (n.d.). Current State of the Sea Ice Cover [Text]. Retrieved March 3, 2018, from https://neptune.gsfc.nasa.gov/csb/index.php?section=234

Curtis, J. A., & Adams, L. J. (1987). Defense Meteorological Satellite Program. *IEEE Aerospace and Electronic Systems Magazine*, *2*(3), 13–17. https://doi.org/10.1109/MAES.1987.5005348

Darby, M. (2018, February 13). Shipping first as commercial tanker crosses Arctic sea route in winter. Retrieved February 15, 2018, from http://www.theguardian.com/environment/2018/feb/13/shipping-first-as-commercial-tanker-crosses-arctic-sea-route-in-winter

Ellis, B., & Brigham, L. (2009). Arctic Marine Shipping Assessment 2009 Report. Retrieved from https://oaarchive.arctic-council.org/handle/11374/54

Fetterer, F., & Knowles, K. (2004). Sea ice index monitors polar ice extent. *Eos, Transactions American Geophysical Union*, *85*(16), 163–163. https://doi.org/10.1029/2004EO160007

Fetterer, F., Knowles, K., Meier, W., Savoie, M., & Windnagel, A. (2017, updated daily). Sea Ice Index, Version 3. NSIDC. https://doi.org/10.7265/N5K072F8

Fisheries and Oceans Canada. (2017, June 8). CHS - Arctic charting. Retrieved March 19, 2018, from http://www.charts.gc.ca/arctic-arctique/index-eng.asp#how_are_seabed

Gagné, M.-è., Kirchmeier-Young, M. C., Gillett, N. P., & Fyfe, J. C. (2017). Arctic sea ice response to the eruptions of Agung, El Chichón, and Pinatubo: ARCTIC SEA ICE RESPONSE TO VOLCANOES. *Journal of Geophysical Research: Atmospheres*, *122*(15), 8071–8078. https://doi.org/10.1002/2017JD027038

Gloersen, P., & Barath, F. (1977). A scanning multichannel microwave radiometer for Nimbus-G and SeaSat-A. *IEEE Journal of Oceanic Engineering*, *2*(2), 172–178. https://doi.org/10.1109/JOE.1977.1145331

Goosse, H., Arzel, O., Bitz, C. M., Montety, A. de, & Vancoppenolle, M. (2009). Increased variability of the Arctic summer ice extent in a warmer climate. *Geophysical Research Letters*, *36*(23). https://doi.org/10.1029/2009GL040546

Guemas, V., Blanchard-Wrigglesworth, E., Chevallier, M., Day, J. J., Déqué, M., Doblas-Reyes, F. J., et al. (2016). A review on Arctic sea-ice predictability and prediction on seasonal to decadal time-scales: Arctic Sea-Ice Predictability

and Prediction. *Quarterly Journal of the Royal Meteorological Society*, *142*(695), 546–561. https://doi.org/10.1002/qj.2401

Holland, M. M., Bitz, C. M., & Tremblay, B. (2006). Future abrupt reductions in the summer Arctic sea ice. *Geophysical Research Letters*, *33*(23). https://doi.org/10.1029/2006GL028024

Holland, M. M., Bailey, D. A., Briegleb, B. P., Light, B., & Hunke, E. (2011). Improved Sea Ice Shortwave Radiation Physics in CCSM4: The Impact of Melt Ponds and Aerosols on Arctic Sea Ice. *Journal of Climate*, *25*(5), 1413–1430. https://doi.org/10.1175/JCLI-D-11-00078.1

Hunke, E., Lipscomb, W., Jones, P., Turner, A., Jeffery, N., & Elliott, S. (2017). *CICE, The Los Alamos Sea Ice Model* (No. CICE; 005315WKSTN00). Los Alamos National Lab. (LANL), Los Alamos, NM (United States). Retrieved from https://www.osti.gov/biblio/1364126

Hurrell, J. W., Holland, M. M., Gent, P. R., Ghan, S., Kay, J. E., Kushner, P. J., et al. (2013). The Community Earth System Model: A Framework for Collaborative Research. *Bulletin of the American Meteorological Society*, *94*(9), 1339–1360. https://doi.org/10.1175/BAMS-D-12-00121.1

Jahn, A., Kay, J. E., Holland, M. M., & Hall, D. M. (2016). How predictable is the timing of a summer ice-free Arctic?: PREDICTING A SUMMER ICE-FREE ARCTIC. *Geophysical Research Letters*, *43*(17), 9113–9120. https://doi.org/10.1002/2016GL070067

Jakobsson, M., Mayer, L., Coakley, B., Dowdeswell, J. A., Forbes, S., Fridman, B., et al. (2012). The International Bathymetric Chart of the Arctic Ocean (IBCAO) Version 3.0. *Geophysical Research Letters*, *39*(12). https://doi.org/10.1029/2012GL052219

Jin, Z. (2004). A parameterization of ocean surface albedo. *Geophysical Research Letters*, *31*(22). https://doi.org/10.1029/2004GL021180

Kay, J. E., Deser, C., Phillips, A., Mai, A., Hannay, C., Strand, G., et al. (2015). The Community Earth System Model (CESM) Large Ensemble Project: A Community Resource for Studying Climate Change in the Presence of Internal Climate Variability. *Bulletin of the American Meteorological Society*, *96*(8), 1333–1349. https://doi.org/10.1175/BAMS-D-13-00255.1

Kwok, R., & Rothrock, D. A. (2009). Decline in Arctic sea ice thickness from submarine and ICESat records: 1958–2008. *Geophysical Research Letters*, *36*(15), L15501. https://doi.org/10.1029/2009GL039035

Labe, Z., Magnusdottir, G., & Stern, H. (2018). Variability of Arctic Sea Ice Thickness Using PIOMAS and the CESM Large Ensemble. *Journal of Climate*, *31*(8), 3233–3247. https://doi.org/10.1175/JCLI-D-17-0436.1

Lamarque, J.-F., Bond, T. C., Eyring, V., Granier, C., Heil, A., Klimont, Z., et al. (2010). Historical (1850–2000) gridded anthropogenic and biomass burning emissions of reactive gases and aerosols: methodology and application. *Atmos. Chem. Phys.*, *10*(15), 7017–7039. https://doi.org/10.5194/acp-10-7017-2010

Lamarque, J.-F., Kyle, G. P., Meinshausen, M., Riahi, K., Smith, S. J., Vuuren, D. P. van, et al. (2011). Global and regional evolution of short-lived radiatively-active gases and aerosols in the Representative Concentration Pathways. *Climatic Change*, *109*(1–2), 191. https://doi.org/10.1007/s10584-011-0155-0

Laxon, S. W., Giles, K. A., Ridout, A. L., Wingham, D. J., Willatt, R., Cullen, R., et al. (2013). CryoSat-2 estimates of Arctic sea ice thickness and volume: CRYOSAT-2 SEA ICE THICKNESS AND VOLUME. *Geophysical Research Letters*, *40*(4), 732–737. https://doi.org/10.1002/grl.50193

Maslanik, J., Stroeve, J., Fowler, C., & Emery, W. (2011). Distribution and trends in Arctic sea ice age through spring 2011. *Geophysical Research Letters*, *38*(13), L13502. https://doi.org/10.1029/2011GL047735

Meier, W. N., Hovelsrud, G. K., van Oort, B. E. H., Key, J. R., Kovacs, K. M., Michel, C., et al. (2014). Arctic sea ice in transformation: A review of recent observed changes and impacts on biology and human activity: ARCTIC SEA ICE: REVIEW OF RECENT CHANGES. *Reviews of Geophysics*, *52*(3), 185–217. https://doi.org/10.1002/2013RG000431

Meinshausen, M., Smith, S. J., Calvin, K., Daniel, J. S., Kainuma, M. L. T., Lamarque, J.-F., et al. (2011). The RCP greenhouse gas concentrations and their extensions from 1765 to 2300. *Climatic Change*, *109*(1–2), 213. https://doi.org/10.1007/s10584-011-0156-z

Melia, N., Haines, K., & Hawkins, E. (2016). Sea ice decline and 21st century trans-Arctic shipping routes: Trans-Arctic shipping in the 21st Century. *Geophysical*

Research Letters, *43*(18), 9720–9728. https://doi.org/10.1002/2016GL069315

Mioduszewski, J. R., Vavrus, S., Wang, M., Holland, M., & Landrum, L. (2018). Future interannual variability of Arctic sea ice in coupled climate models. *The Cryosphere*, *In Review*.

Moore G. W. K. (2012). A climatology of vessel icing for the subpolar North Atlantic Ocean. *International Journal of Climatology*, *33*(11), 2495–2507. https://doi.org/10.1002/joc.3604

Overland, J. E., Hanna, E., Hanssen-Bauer, I., Kim, S.-J., Walsh, J. E., Wang, M., et al. (2017, November 30). Surface Air Temperature. Retrieved February 13, 2018, from http://www.arctic.noaa.gov/Report-Card/Report-Card-2017/ArtMID/7798/ArticleID/700/Surface-Air-Temperature

Perovich, D. K. (2002). Seasonal evolution of the albedo of multiyear Arctic sea ice. *Journal of Geophysical Research*, *107*(C10). https://doi.org/10.1029/2000JC000438

Pithan, F., & Mauritsen, T. (2014). Arctic amplification dominated by temperature feedbacks in contemporary climate models. *Nature Geoscience*, *7*(3), 181–184. https://doi.org/10.1038/ngeo2071

Pizzolato, L., Howell, S. E. L., Dawson, J., Laliberté, F., & Copland, L. (2016). The influence of declining sea ice on shipping activity in the Canadian Arctic: SEA ICE AND SHIPPING, CANADIAN ARCTIC. *Geophysical Research Letters*, *43*(23), 12,146-12,154. https://doi.org/10.1002/2016GL071489

Protection of the Arctic Marine Environment. (2018). Northern Sea Route Shipping Statistics. Retrieved February 15, 2018, from https://pame.is/index.php/projects/arctic-marine-shipping/older-projects/northern-sea-route-shipping-statistics

Pustogvar, A., & Kulyakhtin, A. (2016). Sea ice density measurements. Methods and uncertainties. *Cold Regions Science and Technology*, *131*, 46–52. https://doi.org/10.1016/j.coldregions.2016.09.001

Rodrigue, J.-P. (2017). *The Geography of Transport Systems* (Fourth). New York: Routledge.

Schweiger, A., Lindsay, R., Zhang, J., Steele, M., Stern, H., & Kwok, R. (2011). Uncertainty in modeled Arctic sea ice volume. *Journal of Geophysical Research*, *116*. https://doi.org/10.1029/2011JC007084

Smith, L. C., & Stephenson, S. R. (2013). New Trans-Arctic shipping routes navigable by midcentury. *Proceedings of the National Academy of Sciences*, *110*(13), E1191–E1195. https://doi.org/10.1073/pnas.1214212110

Stephenson, S. R., & Smith, L. C. (2015). Influence of climate model variability on projected Arctic shipping futures: CLIMATE MODEL INFLUENCE ON ARCTIC SHIPPING. *Earth's Future*, *3*(11), 331–343. https://doi.org/10.1002/2015EF000317

Stroeve, J. C., Kattsov, V., Barrett, A., Serreze, M., Pavlova, T., Holland, M., & Meier, W. N. (2012). Trends in Arctic sea ice extent from CMIP5, CMIP3 and

observations. *Geophysical Research Letters*, *39*(16), n/a-n/a. https://doi.org/10.1029/2012GL052676

Taylor, K. E., Stouffer, R. J., & Meehl, G. A. (2012). An Overview of CMIP5 and the Experiment Design. *Bulletin of the American Meteorological Society*, *93*(4), 485–498. https://doi.org/10.1175/BAMS-D-11-00094.1

Timco, G. W., & Kubat, I. (2001). Canadian Ice Regime System: Improvements Using an Interaction Approach. In *Proceedings of the 16th International Conference on Port and Ocean Engineering under Arctic Conditions*.

Timco, G. W., Kubat, I., & Johnston, M. (2005). Scientific Basis for the Canadian Ice Regime System. In *Proceedings of the 18th International Conference on Port and Ocean Engineering under Arctic Conditions*.

Transport Canada. (2010, January 7). Arctic Ice Regime Shipping System (AIRSS) Standards (1998) - TP 12259. Retrieved February 16, 2018, from https://www.tc.gc.ca/eng/marinesafety/tp-tp12259-menu-605.htm

Wadhams, P. (2000). *Ice in the Ocean*. CRC Press.

Zhang, J., & Rothrock, D. A. (2003). Modeling global sea ice with a thickness and enthalpy distribution model in generalized curvilinear coordinates. *Monthly Weather Review*, *131*(5), 845–861.

Zhang, J., Lindsay, R., Schweiger, A., & Steele, M. (2013). The impact of an intense summer cyclone on 2012 Arctic sea ice retreat. *Geophysical Research Letters*, *40*(4), 720–726. https://doi.org/10.1002/grl.50190